Mineralogical Magazine (2022), **86**, 60–77
doi:10.1180/mgm.2021.89

CAMBRIDGE UNIVERSITY PRESS

Article

Cr-pyrope xenocrysts with oxide mineral inclusions from the Chompolo lamprophyres (Aldan shield): Insights into mantle processes beneath the southeastern Siberian craton

Dmitriy I. Rezvukhin[1]*, Evgeny I. Nikolenko[2], Igor S. Sharygin[1,3], Olga V. Rezvukhina[1], Maria V. Chervyakovskaya[4] and Andrey V. Korsakov[1]

[1]Sobolev Institute of Geology and Mineralogy, Siberian Branch of the Russian Academy of Sciences, Novosibirsk 630090, Russia; [2]ALROSA (ZIMBABWE) Ltd., 19 Van Praagh Avenue, Milton Park, Harare, Zimbabwe; [3]Institute of the Earth's Crust, Siberian Branch of the Russian Academy of Sciences, Irkutsk 664033, Russia; and [4]Zavaritsky Institute of Geology and Geochemistry UB RAS, Yekaterinburg, 620016, Russia

Abstract

Pyrope xenocrysts ($N = 52$) with associated inclusions of Ti- and/or Cr-rich oxide minerals from the Aldanskaya dyke and Ogonek diatreme (Chompolo field, southeastern Siberian craton) have been investigated. The majority of xenocrysts are of lherzolitic paragenesis and have concave-upwards (normal) rare earth element (REE_N) patterns that increase in concentration from light REE to medium–heavy REE (Group 1). Four Ca-rich (5.7–7.4 wt.% CaO) pyropes are extremely low in Ti, Na and Y and have sinusoidal REE_N spectra, thus exhibiting distinct geochemical signatures (Group 2). A peculiar xenocryst, s165, is the only sample to show harzburgitic derivation, whilst demonstrating a normal-to-weakly sinusoidal REE_N pattern and the highest Zr (93 ppm) and Sc (471 ppm). Chromite–magnesiochromite, rutile, Mg-ilmenite and crichtonite-group minerals comprise a suite of oxide mineral inclusions in the pyrope xenocrysts. These minerals are characteristically enriched in Cr with 0.6–7.2 wt.% Cr_2O_3 in rutile, 0.7–3.6 wt.% in Mg-ilmenite and 7.1–18.0 wt.% in the crichtonite-group minerals. Complex titanates of the crichtonite group enriched in large ion lithophile elements (LILE) are high in Al_2O_3 (0.9–2.2 wt.%), ZrO_2 (1.5–5.4 wt.%) and display a trend of compositions from the Ca–Sr-specific varieties to the Ba-dominant species (e.g. lindsleyite). In the pyrope xenocrysts the oxides coexist with silicates (clino- and orthopyroxene and olivine), hydrous silicates (talc, phlogopite and amphibole), carbonate (magnesite), sulfides (pentlandite, chalcopyrite, breakdown products of monosulfide and bornite solid solutions), apatite and graphite. *P–T* estimates imply the inclusion-bearing pyrope xenocrysts have been derived from low-temperature peridotite assemblages that resided at temperatures of ~600–800°C and a pressure range of ~25–35 kbar in the graphite stability field. Pyrope genesis is linked to the metasomatic enrichment of peridotite protoliths by Ca–Zr–LILE-bearing percolating fluid–melt phases containing significant volatile components. These metasomatic agents are probably volatile-rich melts or supercritical C–O–H–S fluids that were released from a Palaeo-subduction slab.

Keywords: pyrope, inclusion, crichtonite-group minerals, mantle metasomatism, Chompolo field, Aldan shield

(Received 20 August 2021; accepted 17 November 2021; Accepted Manuscript published online: 12 January 2022; Associate Editor: Makoto Arima)

Introduction

Kimberlite, lamproite and lamprophyre magmas sample a wide variety of xenogenic material from the subcontinental lithospheric mantle. In contrast to olivine and pyroxenes, pyrope and diamond xenocrysts are resistant constituents of mantle material carried to the surface by deep-seated magmas. Their ability to encapsulate mineral inclusions makes them an important source of information even on the deepest domains of the subcontinental lithospheric mantle. Xenocrysts of Cr-pyrope from kimberlites have been employed widely in mantle petrology and geochemistry as well as diamond exploration, providing clues to the composition, structure and evolution of the subcontinental lithospheric mantle (e.g. Gurney and Switzer, 1973; Sobolev *et al.*, 1973; Dawson and Stephens, 1975; Schulze, 1989; Gurney and Zweistra, 1995; Griffin *et al.*, 1999a, 1999b; Pokhilenko *et al.*, 1999; Canil *et al.*, 2003; Grütter *et al.*, 2004, 2006, 2018; Scully *et al.*, 2004; Malkovets *et al.*, 2007; McLean *et al.*, 2007; Kobussen *et al.*, 2009; Ziberna *et al.*, 2013; Shchukina *et al.*, 2016; Rezvukhin *et al.*, 2018; Zhu *et al.*, 2019; Smith, 2020). Much effort has also been made to characterise kimberlitic diamonds and their associated inclusions (see reviews in Stachel and Harris, 2008; Shirey *et al.*, 2013). These studies have significantly improved our knowledge of the processes occurring in the lithospheric mantle of ancient cratons and contributed to the progress of mantle geoscience. Another insightful approach might be to study the mantle from the view of inclusions hosted by Cr-pyrope. As yet, however, minerals embedded in Cr-pyrope xenocrysts from deep-sourced magmatic rocks (especially other

*Author for correspondence: Dmitriy I. Rezvukhin, Email: m.rezvukhin@igm.nsc.ru, m.rezvukhin@gmail.com

Cite this article: Rezvukhin D.I., Nikolenko E.I., Sharygin I.S., Rezvukhina O.V., Chervyakovskaya M.V. and Korsakov A.V. (2022) Cr-pyrope xenocrysts with oxide mineral inclusions from the Chompolo lamprophyres (Aldan shield): Insights into mantle processes beneath the southeastern Siberian craton. *Mineralogical Magazine* **86**, 60–77. https://doi.org/10.1180/mgm.2021.89

than kimberlites) have received only limited attention. In seeking to understand the genesis of pyrope in the subcontinental lithospheric mantle and address the problem of garnet modification by metasomatic liquids, it is desirable to study mineral inclusions in Cr-pyrope samples from various occurrences of deep-seated mantle rocks the world over.

Available mineralogical data indicate the Cr-pyrope of the lherzolitic paragenesis as being the principal host for a series of Ti-rich oxide inclusions namley: rutile, Mg-rich ilmenite ('picroilmenite'), crichtonite-group minerals, srilankite and carmichaelite (Botkunov *et al.*, 1987, Kostrovitsky and Garanin, 1992, Wang *et al.*, 1999; Săbău and Alberico, 2003; Vrana, 2008; Alifirova *et al.*, 2012, 2020; Ziberna *et al.*, 2013; Nikolenko *et al.*, 2017, 2021; Rezvukhin *et al.*, 2018, 2019). Although there is characteristic enrichment in Ti and Fe, these oxide phases also contain elevated amounts of silicate-incompatible elements, such as high-field-strength elements (HFSE: Nb, Zr and Ta) in rutile, Zr in srilankite, and an exotic array of large ion lithophile elements (LILE: Ba, Sr and K), HFSE, and light rare earth elements (LREE: La, Ce) in the crichtonite-group minerals. These compositional characteristics are atypical compared to depleted peridotites of the subcontinental lithospheric mantle, which are considered as representing a residue after high degrees of melt extraction (e.g. Boyd, 1989; Walter, 1998; Griffin *et al.*, 2003; Doucet *et al.*, 2012). The distinctive compositions of inclusions associated with Cr-pyrope (i.e. enrichment in incompatible elements) might indicate the metasomatic origin of some lherzolitic garnets in the lithospheric mantle of ancient cratons, as suggested previously (e.g. Hoal *et al.*, 1994; Griffin *et al.*, 1999c; Stachel *et al.*, 2004; Howarth *et al.*, 2014).

The Aldan shield (southeastern Siberian craton) is a geological structure of prime interest with regard to a rich diversity of alkaline magmatic rocks exposed in the area. Although the scientific possibilities to explore these rocks have been hindered by their remoteness and inaccessibility, research of the petrology and geochemistry of lamproites, carbonatites and complex alkaline massifs has been carried out (e.g. Makhotkin *et al.*, 1989; Bogatikov *et al.*, 1991; Mitchell *et al.*, 1994; Mues-Schumacher *et al.*, 1995, 1996; Kornilova, 1997; Vladykin, 1997, 2009; Davies *et al.*, 2006; Nikolenko *et al.*, 2020b). The studies of lamproites, which are the dominant deep-seated rocks of mantle origin within the Aldan shield, were partly stimulated by the discovery of diamondiferous lamproites in West Kimberley, Western Australia (Jaques *et al.*, 1984) and Prairie Creek, USA (Smith and Skinner, 1984). The subcontinental lithospheric mantle beneath the Aldan shield remains one of the least studied mantle sections within the Siberian craton, because xenogenic material of deeply-sourced rocks has been given a much lower priority compared to the host rocks. Apart from a few reports dealing with mantle-derived garnet and clinopyroxene xenocrysts from the Chompolo and Tobuk–Khatystyr fields (Kostrovitsky and Garanin, 1992; Varlamov *et al.*, 1996; Ashchepkov *et al.*, 2001; Nikolenko *et al.*, 2017, 2021; Alifirova *et al.*, 2020) and a series of investigations devoted to the xenoliths occurring in alkali basalts from Tok, Stanovoy terrane, southern Aldan shield (Ionov *et al.*, 2005; Tommasi *et al.*, 2008 and references therein), little is known of the composition, structure and thermal state of the lithospheric mantle beneath the Aldan shield. Located in the Central Aldan, lamprophyres of the Chompolo field are a valuable source of information concerning mantle parageneses as they contain abundant Cr-pyrope xenocrysts with associated mineral inclusions of remarkable diversity: Ti–Cr-rich oxides, silicates, carbonates, sulfides, hydrous minerals, graphite and composite polymineralic inclusions (Kostrovitsky and Garanin, 1992; Nikolenko *et al.*, 2017, 2021; Alifirova *et al.*, 2020; this study).

This contribution reports detailed mineralogical and geochemical data for pyrope xenocrysts with oxide inclusions from the Aldanskaya dyke and Ogonek diatreme, two lamprophyre bodies of the Chompolo field. In the discussion we provide *P*–*T* estimates for the samples investigated, compare inclusion composition with existing data for Ti-oxide minerals from the lithospheric mantle, and make an attempt to constrain the nature of the melts/fluids that gave rise to crystallisation of the xenocryst mineral suite. The Aldan shield represents a craton–margin setting that has been affected by a series of subduction episodes, accompanied by crustal thinning (e.g. Ionov *et al.*, 2005; Khomich *et al.*, 2015). On a global scale, our data might have implications for metal transfer and ore-forming processes in craton–margin settings affected by subduction (Holwell *et al.*, 2019), and for the role of the continental lithosphere in Earth's volatile cycle (Gibson *et al.*, 2020).

Geological setting

The Siberian craton occupies an area of 4×10^6 km^2. It is composed of Archean and Proterozoic microcontinents (terranes) that underwent final amalgamation at ca. 1.9 Ga (Rosen *et al.*, 1994; Rosen and Turkina, 2007; Smelov and Timofeev, 2007; Paquette *et al.*, 2017; Donskaya, 2020). The major part of the craton (~70%) is covered by a thick (1–8 km) layer of Phanerozoic sedimentary rocks. The exposures of crystalline basement are related to tectonic uplifts and comprise <30% of the craton area. The Aldan Shield is the largest (350×1200 km) exposure of the Siberian craton. This crops out at the southeast part of the shield and consists of several terranes, which are bounded by faults and collisional suture zones (Fig. 1) (Smelov and Timofeev, 2005). As a consequence of intense magmatic activity throughout its geological history, the Aldan shield contains numerous major ore deposits of uranium, gold, platinoids and rare metals formed during the Early Precambrian to Late Mesozoic, as well as ultramafic- and mafic-alkaline plutons, lamproites, and lamprophyres (Smelov and Timofeev, 2005; Khomich *et al.*, 2015). The Central Aldan superterrane consisting of the Nimnyr and Sutam terranes is a stable granulite–gneiss ancient cratonic domain of the Aldan shield, though it experienced an intense Mesozoic tectono–magmatic reworking accompanied by a pronounced alkaline magmatism (Bogatikov *et al.*, 1991).

The Chompolo lamprophyres belong to the Aldan alkaline suite of rocks which also comprises alkaline massifs with lamproite occurrences (Murun, Lomam, Yakokut, Inagli, Tommot, Bilibin, Konder and others), lamproite pipes and dykes (e.g. Kayla, Molbo and Khani), diatremes of the Tobuk–Khatystyr field and numerous alkaline/subalkaline dykes and sills (Bogatikov *et al.*, 1991, 1994; Vladykin, 1997; Davies *et al.*, 2006). The Chompolo area is a part of the Central Aldan superterrane and lies within the Amga collision suture zone between the West Aldan granite–greenstone composite terrane and Nimnyr granulite–orthogneiss terrane (Smelov and Timofeev, 2005) (Fig. 1). The Aldanskaya dyke was discovered in 1957 and other magmatic bodies of the Chompolo field were found soon after. Initial studies classified the Chompolo mantle-derived rocks as kimberlites (Shilina and Zeitlin, 1959); but they have been re-classified subsequently as lamproites (e.g. Bogatikov

https://doi.org/10.1180/mgm.2021.89 Published online by Cambridge University Press

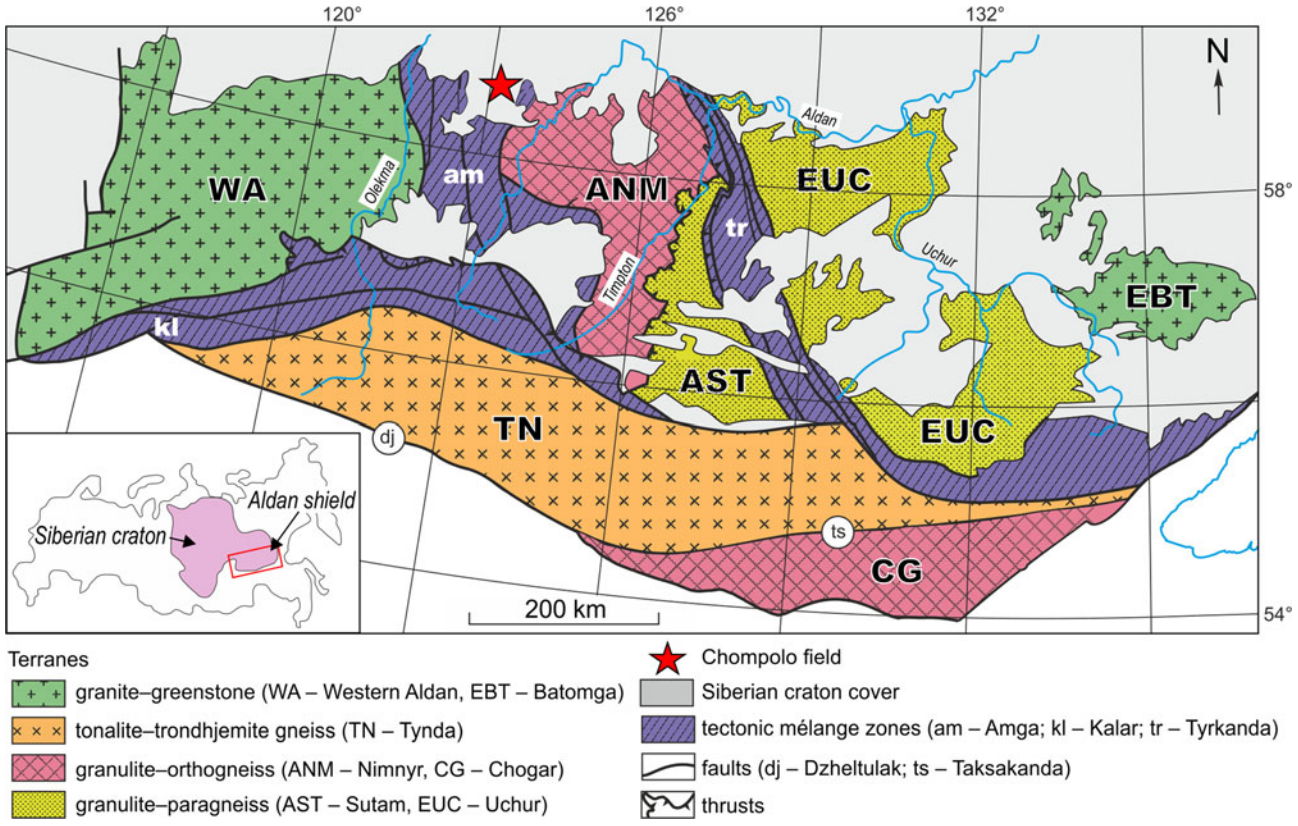

Fig. 1. Tectonic sketch map of the Aldan shield. Inset shows location of the Aldan shield within the Siberian craton. Modified after (Smelov *et al.*, 2012).

et al., 1991) or lamprophyres (Kornilova, 1997; Nikolenko *et al.*, 2020b). Here we will refer to the Chompolo intrusions as lamprophyres on the basis of the most recent and accurate petrographic descriptions by Kornilova (1997) and Nikolenko *et al.* (2020b). Within the Chompolo district, there are six pipes (Ogonek, Gornaya, Perevalnaya, Sputnik, Intrusions No. 29 and No. 104), two dykes (Aldanskaya, Kilier) and veins Osenniye (Vladimirov *et al.*, 1989). All of these lamprophyre bodies vary significantly in size (e.g. the Aldanskaya dyke covers 800 m × 25 m; Ogonek pipe – 100 m × 80 m; Gornaya pipe – 100 m × 40 m). The Chompolo lamprophyres consist of clastic tuff breccia, in addition the diatremes Perevalnaya and Intrusion No. 104 exhibit massive textures (Kornilova, 1997). Abundant (30–70 vol.%) xenogenic fragments are dominated by xenoliths of metamorphic rocks and xenocrysts of upper mantle origin (pyrope, diopside, enstatite, chromium spinel, phlogopite and Mg-rich ilmenite) (Kornilova, 1997; Nikolenko *et al.*, 2020b). The majority of mantle-derived xenoliths are extensively weathered and disintegrated.

The lamprophyres of the Chompolo field are poorly characterised and for most of these rocks isotopic age determinations are not available. Until recently, the age only of Intrusion No. 104 was available (131 ± 4 Ma, Rb–Sr isochron ages of phlogopite; Zaitsev and Smelov, 2010). Nikolenko *et al.* (2020b) provided additional age constraints for the Aldanskaya dyke (157.0 ± 1.6 Ma) and Ogonek diatreme (137.8 ± 1.2 Ma) on the basis of K-richterite Ar–Ar radiometric ages. For the lamprophyre sills located in the nearby Upper Amga alkaline complex, ages in the range of ca. 117–135 Ma have been determined (Ar–Ar radiometric ages of phlogopite and K-feldspar; Prokopyev *et al.*, 2019 and references therein). The Chompolo rock occurrences are probably related to the extensive magmatic events that were widespread within the Central Aldan between ca. 175 and 120 Ma (Bogatikov *et al.*, 1991; Ivanov *et al.*, 2018). The available K–Ar ages of phlogopite constrained the age of the Aldan lamproites at 147–120 Ma, except for the Khani ones located in the Western Aldan which are Proterozoic (1.8–1.9 Ga) (Makhotkin *et al.*, 1989; Bogatikov *et al.*, 1991; Mues-Schumacher *et al.*, 1995, 1996; Vladykin, 1997).

Samples and methods

Garnet xenocrysts were sampled from exploration trenches and pits within the Chompolo lamprophyre bodies and examined using optical microscopy. The majority of garnets in the concentrate population (sieve class 2–4 mm) are intense red in colour, with minor amounts of orange species presumably of eclogitic or pyroxenitic paragenesis. Note that some of the orange and red garnets contain a characteristic network of regularly spaced and preferentially oriented thin (0.1–3 μm) lamellae of rutile (and perhaps silicates), which might be of solid-state exsolution origin. During hand-picking we tried to avoid garnets with such preferentially oriented dense frameworks of inclusions and focused on xenocrysts with larger encapsulated minerals suitable for microprobe analysis. The occurrence of dark-coloured oxide inclusions of appreciable size (>10 μm in smallest dimension) was the primary criterion for sample selection. The pyrope crystals containing relevant inclusions were mounted in epoxy resin and subsequently ground and polished to expose the inclusions on the surface. This investigation is based on a subset of 48 Cr-pyrope xenocrysts from the Aldanskaya dyke and four crystals

https://doi.org/10.1180/mgm.2021.89 Published online by Cambridge University Press

from the Ogonek diatreme. On the basis of visual inspection of hundreds of garnet grains from the Chompolo rocks, we argue that this set of samples is representative enough to cover all possible inclusion textures in Chompolo pyropes and a major range of garnet and oxide mineral compositions.

Back-scattered electron (BSE) images and preliminary compositional data were acquired using a Tescan MIRA 3 LMU scanning electron microscope (SEM) equipped with an INCA 450+ XMax-80 X-ray energy-dispersive spectroscopic (EDS) system (Oxford Instruments). A JEOL JXA-8100 electron microprobe (EMP) was employed to perform quantitative analyses of major elements in minerals. The SEM-EDS and EMP analytical procedures were undertaken at the Analytical Center for Multi-elemental and Isotope Research, Sobolev Institute of Geology and Mineralogy, Siberian Branch of the Russian Academy of Sciences (IGM SB RAS). Analytical conditions on the EMP instrument were a 20 kV accelerating voltage, 20 nA current (100 nA for crichtonite-group minerals), ~1–2 μm beam diameter, and spectrum acquisition times of 20–50 s for peak and background. Several spots on each garnet were analysed to determine homogeneity. A number of natural and synthetic standards were used. *ZAF* and *CITZAF* matrix corrections were applied. The standards employed for routine calibration and instrument stability monitoring were garnet (O-145), ilmenite (GF-55), rutile (TiO_2), chromite (79/62) and several synthetic compounds, e.g. Ba- and Sr-doped glasses. Particular attention was given to the overlap corrections for Ti and V, Ti and Ba, Ti and Ce, Ba and Ce when analysing the oxide minerals. Limits of detection were 0.01–0.04 wt.% oxide. Estimated precision of the analyses was below 1–2% for major and below 5% for minor oxides. In order to avoid signal contributions from the host garnet, EMP analyses of inclusions were performed on exposed grains with diameter ≥10 μm. To check for possible host garnet contribution Si was included in the sets of analysed elements. A few analyses of oxide inclusions with SiO_2 concentration >0.4 wt.% were rejected from the database.

Confocal Raman spectroscopy was carried out in several samples to identify minerals within unexposed inclusions to provide better representation of the inclusion associations in the xenocrysts. The Raman spectra were collected using a Horiba Jobin Yvon LabRAM HR800 Raman microspectrometer equipped with a 532-nm Nd:YAG laser and an Olympus BX41 microscope at IGM SB RAS. The spectra were acquired at room temperature in back-scattered geometry with a spectral resolution of ~2 cm^{-1}. The system was calibrated using the 520.7 cm^{-1} Raman band of a silicon wafer before and after each experimental session. The RRUFF project database (http://rruff.info/; Lafuente *et al.*, 2015) and *CrystalSleuth* application (Laetsch and Downs, 2006) were used for mineral identification.

The trace-element composition of the garnets (29 elements, including Na, Zr, Y, Sc, V, U, Th, Pb, Ni, Ba, Sr, Ti, Nb, Ta, Hf and REE) was determined *in situ* by laser ablation-inductively coupled plasma-mass spectrometry (LA-ICP-MS) at Zavaritsky Institute of Geology and Geochemistry (Analytical center "Geoanalitik", Ural Branch of the Russian Academy of Sciences). An ESI NWR 213 nm laser ablation system was coupled to a PerkinElmer NexION 300S quadrupole mass spectrometer. The garnets were ablated by a laser pulsed at 10 Hz with an energy of 10.5–11.5 J/cm^2. Helium was used as carrier gas at ~400 ml/min flow and data were acquired in time resolved mode. Generally, one spot per garnet was analysed and the diameter of the resulting crater was ~50 μm. The NIST SRM 612 multi-element glass was used as a primary standard, whereas the CaO concentration (wt.%) in garnet was used as an internal standard. Each block of analyses consisted of measuring 10 unknowns preceded and followed by measuring the NIST glass. Detection limits were below 0.1 ppm for most elements (99% confidence), with the exception of Sc, Ti, V, Ni (considerably below 1 ppm) and Na (~1 ppm). Analytical precision was better than 8% (1σ). The individual measurements were normalised and reduced to concentrations using *GLITTER* software v. 4.4 (Griffin *et al.*, 2008).

Mineralogy and textures of inclusions

All the pyrope xenocrysts investigated host oxide mineral inclusions and oxide-bearing polymineralic assemblages. A summary of samples is shown in Table 1, representative photographs of the pyrope xenocrysts are given in Fig. 2, and the inclusion textures in Fig. 3. The pyrope xenocrysts are irregular in shape and range in size from 2 to 4 mm. Most pyropes are devoid of kelyphitic rims. Rutile, Mg-rich ilmenite and crichtonite-group minerals (Ti-rich oxide suite) are the most abundant enclosed minerals in the Chompolo pyropes and are associated commonly with each other (Table 1), forming euhedral needle-, rod- and blade-like prismatic inclusions, with a typical diameter of 5–30 μm and length up to 2 mm. Mg-ilmenite and crichtonite-group minerals also form lamellae and thin (<10 μm) platy grains. Several grains of Ti-rich oxides exceed 100 μm in the smallest dimension. Large (>20 μm) rutile inclusions typically contain fine (<1 μm) ilmenite lamellae (e.g. Fig. 3e). The quantity of the elongated Ti-rich oxide grains in the xenocrysts is estimated to vary from several dozens to two hundred. The rutile needles are orange–mauve in colour and are semi-transparent, whereas the inclusions of Mg-rich ilmenite and crichtonite-group minerals are jet-black and opaque (Fig. 2), being semi-transparent only in very thin slices. Typically, the elongated inclusions of the Ti-oxides are oriented in host pyrope along specific directions (Fig. 2). Large inclusions of Cr-spinel (up to 300 μm) are located separately from the Ti-oxides in distinct xenocrysts (Fig. 2g–i), where they are either octahedral or show more complex morphology with an increased number of facets. Composite associations of Ti-oxides and Cr-spinel appear in several samples; in such cases Cr-spinel is a smaller mineral (10–50 μm; Fig. 3f).

Within individual pyrope xenocrysts, the oxide inclusions are commonly associated with silicates (clino- and orthopyroxene and olivine), hydrous silicates (talc, phlogopite and amphibole), carbonate (magnesite), sulfides (pentlandite, chalcopyrite, breakdown products of monosulfide and bornite solid solutions), apatite and graphite (Table 1). Among the silicate minerals, olivine and Cr-diopside predominate, and only two grains of enstatite were found: (1) as an intergrowth with Cr-diopside and (2) as a grain in a composite polymineralic inclusion. Intergrowths of the oxides with each other and with the silicates are abundant (Fig. 3). For example, in xenocryst ALD-1-6 seven intergrowths of various modal compositions have been recognised within a single pyrope (see Fig. 3 and Table 1 for specific associations). Fe-rich talc occurs abundantly as individual inclusions or as intergrowths with the Ti-oxides (Fig. 3j). Talc is never associated with cracks extending to the edge of the host, implying its syngenetic origin. Four pyrope xenocrysts contain rounded or irregularly-shaped complex polymineralic intergrowths, where oxides (rutile, Mg-rich ilmenite, crichtonite-group minerals and Cr-spinel) comprise characteristic composite aggregates with silicates (enstatite), hydrous silicates (phlogopite, amphibole), sulfides and carbonate (magnesite).

https://doi.org/10.1180/mgm.2021.89 Published online by Cambridge University Press

Table 1. Summary of sample data.

Sample	Site	Group	Paragenesis[a]	Ni (ppm) [b]	T_{Ni} (°C) [c]	P^{d}_{Ca-Cr}	Inclusion associations*
ALD-1-1	Aldanskaya	1	G9	13	712	24	Rt+Ilm+CGM+Cpx+(Ilm+Dol)
ALD-1-2	Aldanskaya	1	G9	13	700	**29**	Rt+Ilm+CGM+Ol+(Rt+Spl)+(Rt+Ol)+(Spl+Talc) +(Spl+Talc)+(Cpx+Talc)+Talc
ALD-1-3	Aldanskaya	1	G9	14	720	26	Rt+Ilm+CGM+(Rt+Ilm)
ALD-1-4	Aldanskaya	1	G9	12	689	30	Rt+CGM+(Rt+Ol)+(Rt+CGM+Cpx+Talc)+(Cpx+Opx)
ALD-1-5	Aldanskaya	1	G9	14	723	24	Rt+Ilm+CGM
ALD-1-6	Aldanskaya	1	G9	13	710	**27**	Rt+Ilm+CGM+(Rt+Ilm)+(Rt+CGM)+(Rt+Ol) +(Rt+Ilm+Ol)+(Rt+Talc)+(Rt+Cpx+Talc)+(Ilm+Spl)
ALD-1-7	Aldanskaya	1	G9	14	721	31	Rt+CGM+(Rt+Ol)
ALD-1-8	Aldanskaya	1	G9	12	689	24	Rt+Ilm+CGM+(Rt+Ilm)
ALD-1-9	Aldanskaya	1	G9	14	714	26	Rt+Ilm+CGM+(Rt+Ilm)
ALD-1-10	Aldanskaya	1	G9	13	701	30	Rt+CGM+(Rt+Ilm+CGM)
ALD-1-11	Aldanskaya	1	G9	15	733	27	Rt+Ilm+CGM+(Rt+Ilm+Ol)
ALD-1-12	Aldanskaya	1	G9	9	646	21	Rt+Ilm
ALD-1-13	Aldanskaya	1	G9	12	694	27	Rt+Ilm+CGM
ALD-1-14	Aldanskaya	1	G9	13	706	29	Rt+Ilm+CGM+Dol
ALD-1-15	Aldanskaya	1	G9	13	713	26	Rt+CGM+(Rt+Ilm+Phl)+(Rt+Talc)
ALD-1-16	Aldanskaya	1	G9	15	733	27	Rt+Ilm+(Rt+Ol)
ALD-2-C	Aldanskaya	2	G12	10	655	**25**	Spl
ALD-3-1	Aldanskaya	2	G9	11	680	**27**	Spl
ALD-3-2	Aldanskaya	1	G9	12	688	25	Rt+Ilm+CGM
ALD-3-3	Aldanskaya	2	G9	12	695	**27**	Spl
ALD-3-4	Aldanskaya	2	G9	11	676	**27**	Spl
ALD-3-5	Aldanskaya	–	G9	14	723	**30**	Spl
ALD-3-6	Aldanskaya	1	G9	11	671	23	Rt+Ilm+CGM
ALD-3-7	Aldanskaya	1	G9	13	706	28	Rt+CGM
ALD-4-1	Aldanskaya	1	G9	10	668	21	Rt+Ilm
ALD-4-2	Aldanskaya	1	G9	11	679	28	Rt+(Rt+Ilm)+(Rt+Ilm+Talc)
ALD-4-3	Aldanskaya	1	G9	10	662	30	Rt+Ilm
ALD-4-4	Aldanskaya	1	G9	9	642	29	Rt+Ilm
ALD-4-5	Aldanskaya	1	G9	14	717	24	Rt+CGM
ALD-4-6	Aldanskaya	1	G9	12	695	28	Rt+Ilm
ALD-4-7	Aldanskaya	1	G9	13	709	30	Rt+Ilm
ALD-4-8	Aldanskaya	1	G9	10	667	23	Rt+Ilm
ALD-4-9	Aldanskaya	1	G9	15	735	28	Rt+Ilm+CGM
ALD-4-10	Aldanskaya	1	G9	14	724	26	Rt+CGM
ALD-4-11	Aldanskaya	1	G9	11	678	**30**	Rt+Ilm+(Spl+Cpx)
ALD-4-12	Aldanskaya	1	G9	12	684	29	Rt+Ilm+CGM+(Rt+Ilm)
ALD-4-13	Aldanskaya	1	G9	15	736	27	Rt+Ilm
ALD-4-14	Aldanskaya	1	G9	11	671	30	Rt+Ilm
ALD-4-15	Aldanskaya	1	G9	16	748	31	Rt+CGM
ALD-4-16	Aldanskaya	1	G9	14	725	29	Rt+Ilm+CGM
ALD-4-17	Aldanskaya	1	G9	15	739	26	Rt+Ilm
ALD-4-18	Aldanskaya	1	G9	13	701	31	Rt+Ilm
s3	Aldanskaya	1	G9	13	705	20	Rt+Ilm+(Rt+Ilm)+(Rt+Talc)
s21	Aldanskaya	1	G9	13	706	29	Mgs+Cpx+Phl+Gr+(CGM+Ol)+(CGM+Mgs)
s22	Aldanskaya	1	G9	14	722	24	Rt+Ilm+(Rt+Talc)+(Ilm+Talc)+(Ilm+Cpx)
sx2	Aldanskaya	1	G9	13	711	**26**	(Rt+Spl+Amp+Opx+Mss+Btss+Ccp)
1n11	Aldanskaya	1	G9	15	731	25	Rt+Ilm+CGM+Amp+Ol+Gr+Ccp+(Rt+Cpx+Ap+Mgs)
s165	Aldanskaya	–	G10	15	735	**33**	Spl+Talc+Phl
s291	Ogonek	1	G9	13	702	**28**	(CGM+Spl+Amp+Phl+Mgs+Mss+Pn+Ccp)
s307	Ogonek	1	G9	16	747	32	Rt+CGM+(Rt+CGM+Cpx)+(Rt+Ol)
s317	Ogonek	1	G9	10	666	**26**	(Rt+CGM+Spl+Phl+Mgs+Btss)
s328	Ogonek	1	G9	16	741	26	Rt+Ilm+CGM

[a]After Grütter *et al.* (2004); [b] Ni concentrations are rounded to whole numbers; [c] after Ryan *et al.* (1996); [d] after Grütter *et al.* (2006). Pressure values for samples with spinel inclusions are indicated in bold. For other samples the values are minimum pressures (Grütter *et al.*, 2006).
* Minerals in brackets are intergrowths and complex polymineralic inclusions. Amp – amphibole, Ap – apatite, Btss – bornite solid solution, Ccp – chalcopyrite, CGM – crichtonite group mineral, Cpx – clinopyroxene, Gr – graphite, Grt – garnet, Ilm – Mg-rich ilmenite, Mgs – magnesite, Mss – monosulfide solid solution, Ol – olivine, Opx – orthopyroxene, Phl – phlogopite, Pn – pentlandite, Rt – rutile, Spl – Cr-spinel.

These complex inclusions contain six to eight different minerals (see Table 1 and Fig. 3 for specific associations).

Garnet compositions

Microprobe determined compositions show that individual garnet grains are homogeneous, except for minor diffusional halos around large Cr-spinel inclusions. All the garnets are chromium pyropes with Mg# = 100×Mg/(Mg + Fe) varying from 73.6 to 84.4. Bivariate and normalised trace-element distribution plots illustrating the composition of the xenocrysts are shown in Fig. 4 and Fig. 5, respectively. Major- and trace-element compositions are given in Supplementary Table S1. Strontium concentrations in all the samples are low (<< 2 ppm). Nickel contents are relatively low and vary only from 8.9 to 16.3 ppm. Niobium and Ta abundances are below primitive mantle and TiO_2 levels do not exceed 0.40 wt.%.

https://doi.org/10.1180/mgm.2021.89 Published online by Cambridge University Press

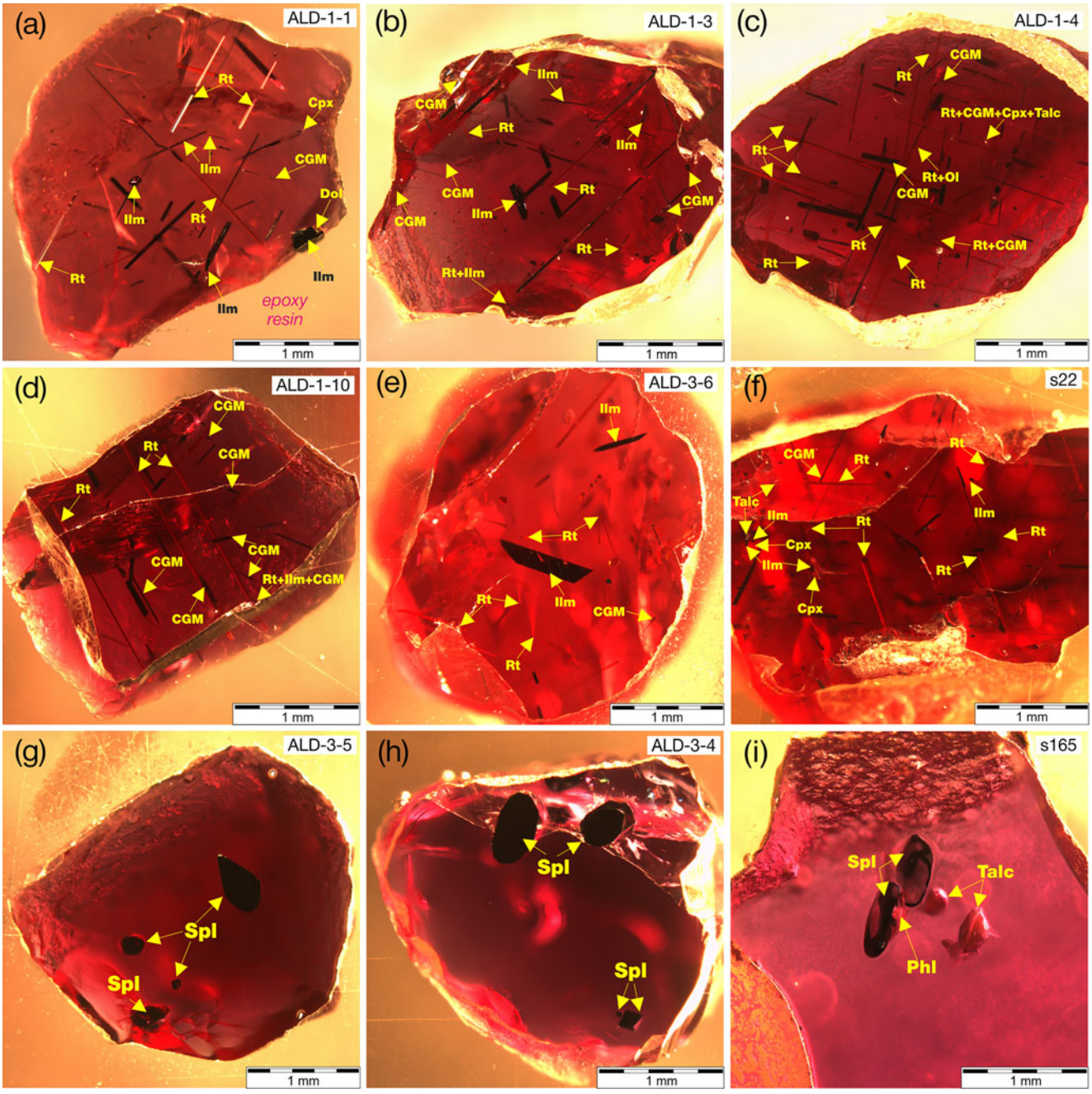

Fig. 2. Photomicrographs of polished pyrope xenocrysts with oxide mineral inclusions from the Chompolo lamprophyres. Rt – rutile, Ilm – Mg-rich ilmenite ('picroilmenite'), CGM – crichtonite group mineral, Spl – Cr-spinel, Cpx – clinopyroxene, Ol – olivine, Phl – phlogopite, Dol – dolomite.

On the basis of major- and trace-element compositions and inclusion assemblages, the garnet xenocryst suite can be classified into four groups.

Group 1

Group 1 comprises the majority of samples ($N = 42$) from Aldanskaya and all four garnets from Ogonek. These garnets exhibit the composition typical for lherzolitic (G9) pyropes (Sobolev *et al.*, 1973; Grütter *et al.*, 2004) with Cr_2O_3 concentrations between 1.93 and 6.35 wt.% and CaO between 4.36 and 6.28 wt.% (Fig. 4a). The Mg# in pyropes of Group 1 lies in the interval 74.0–80.9. Titanium concentrations range from 856 to 2301 ppm and Na content is 157–532 ppm. MnO varies from 0.43 to 0.68 wt.%. Group 1 garnets feature the convex-upward medium–heavy rare earth element (M–HREE) enriched (normal) chondrite-normalised REE distribution patterns (Fig 5b), which are common for fertile lherzolitic garnets worldwide (e.g. Stachel *et al.*, 1998). The chondrite-normalised concentrations rise steeply from La to Sm, whereas from Sm to Lu the patterns are relatively horizontal (unfractionated) with absolute concentrations at 3–30 times chondrite values (McDonough and Sun, 1995). In Group 1 pyropes the Zr concentrations range from 2 to 82 ppm and Y contents are 5–39 ppm. These xenocrysts exhibit

https://doi.org/10.1180/mgm.2021.89 Published online by Cambridge University Press

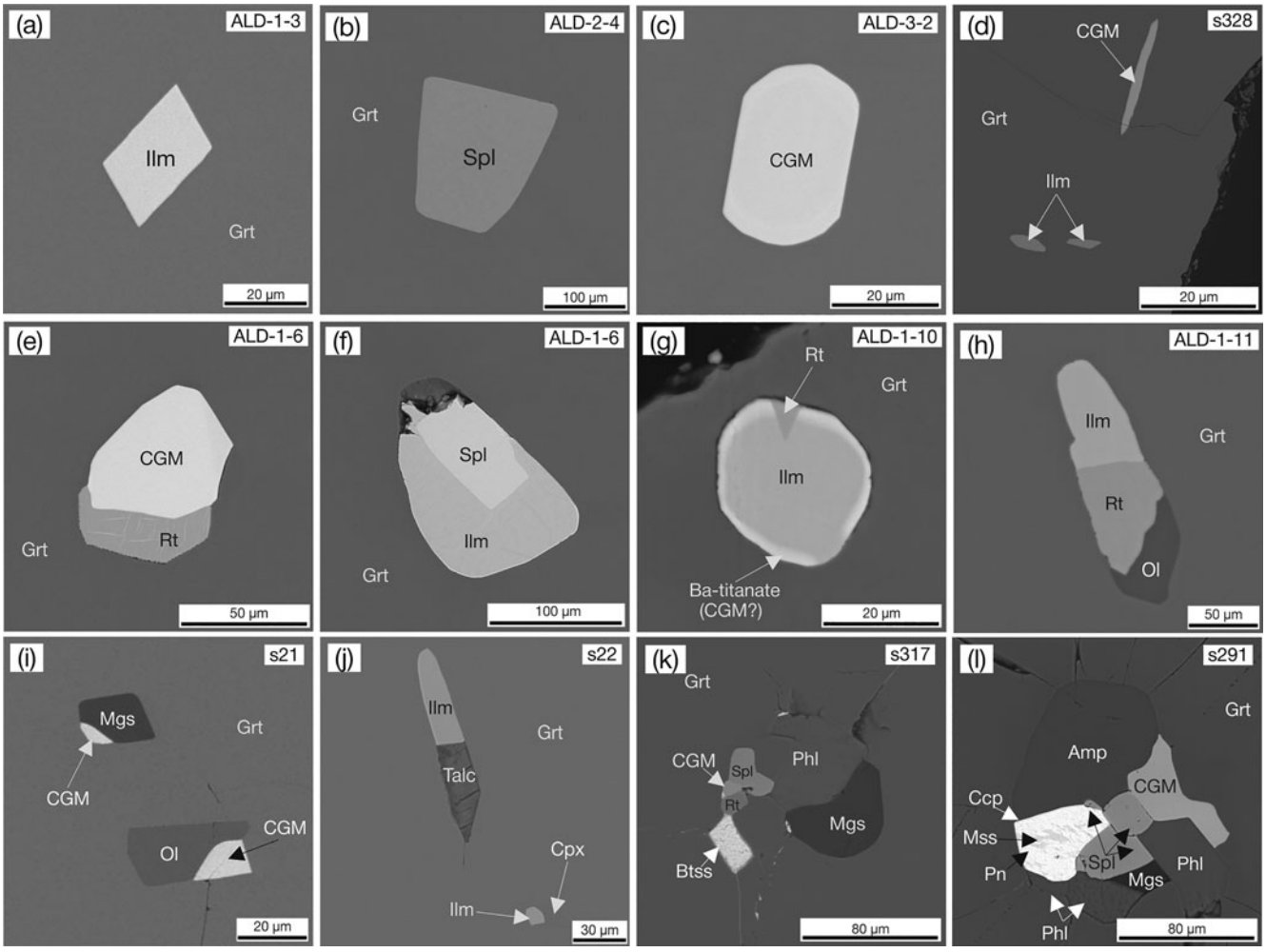

Fig. 3. Back-scattered electron images showing monomineralic (a–d) and polymineralic (e–l) inclusions in Chompolo pyropes. Amp – amphibole, Btss – bornite solid solution, Ccp – chalcopyrite, CGM – crichtonite group mineral, Grt – garnet, Ilm – Mg-rich ilmenite, Mgs – magnesite, Mss – monosulfide solid solution, Ol – olivine, Opx – orthopyroxene, Phl – phlogopite, Pn – pentlandite, Rt – rutile, Spl – Cr-spinel.

a wide range of V concentrations (130–382 ppm) and V/Sc ratios (0.95–2.73). Ti-rich oxides as well as silicate, sulfide, carbonate minerals and composite polymineralic inclusions are indicative of pyropes of this group.

Group 2

Group 2 includes four pyropes from Aldanskaya. These garnets belong to lherzolitic ($N = 3$) and wehrlitic ($N = 1$) parageneses according to Sobolev *et al.* (1973) and Grütter *et al.* (2004). Garnets of Group 2 are relatively high in CaO (5.74–7.42 wt.%) and contain very similar Cr_2O_3 content at 4.84–4.95 wt.% (Fig. 4a). MnO abundances fall near the high end at 0.61–0.66 wt.%. Interestingly, garnets of Group 2 display LREE-enriched sinusoidal chondrite-normalised REE patterns (Fig 5b). A prominent feature of these samples is very low concentrations of Ti (219–351 ppm), Na (83–134 ppm) and Y (<2 ppm). Zr in garnets of Group 2 varies from 3 to 36 ppm, and these samples plot either within, or immediately near, the field of depleted garnets established by Griffin and Ryan (1995) in Zr–Y space (Fig. 4b). Group 2 xenocrysts are characterised by relatively low V abundances (130–219 ppm) and low V/Sc ratios (0.72–1.37). These pyrope grains lack Ti-oxide inclusions and enclose individual grains of Cr-spinel significantly larger (100–300 μm) than those in pyropes of Group 1 (10–50 μm). Group 2 samples are thus readily distinguished from garnets of Group 1 on the basis of both distinctive composition and inclusion associations.

ALD-3-5

A single garnet (ALD-3-5; Aldanskaya) with the lowest Mg# (73.6) combines the characteristic features of Group 1 and Group 2 samples. It is relatively high in both CaO and Cr_2O_3 (6.98 wt.% and 6.34 wt.%, respectively, and thus straddles the lherzolite–wehrlite boundary) (Fig. 4a) and shows a normal chondrite-normalised REE distribution pattern (Fig 5b). However, it is very low in Na (76 ppm) and V/Sc (1.43), is higher in LREE than Group 1 samples and encloses large inclusions of Cr-spinel. ALD-3-5 can be considered as intermediate between Group 1 and Group 2, suggesting the existence of a petrogenetic link relating these two populations.

s165

A single xenocryst (s165; Aldanskaya) with inclusions of Cr-spinel, talc and phlogopite is the only sample to show a

https://doi.org/10.1180/mgm.2021.89 Published online by Cambridge University Press

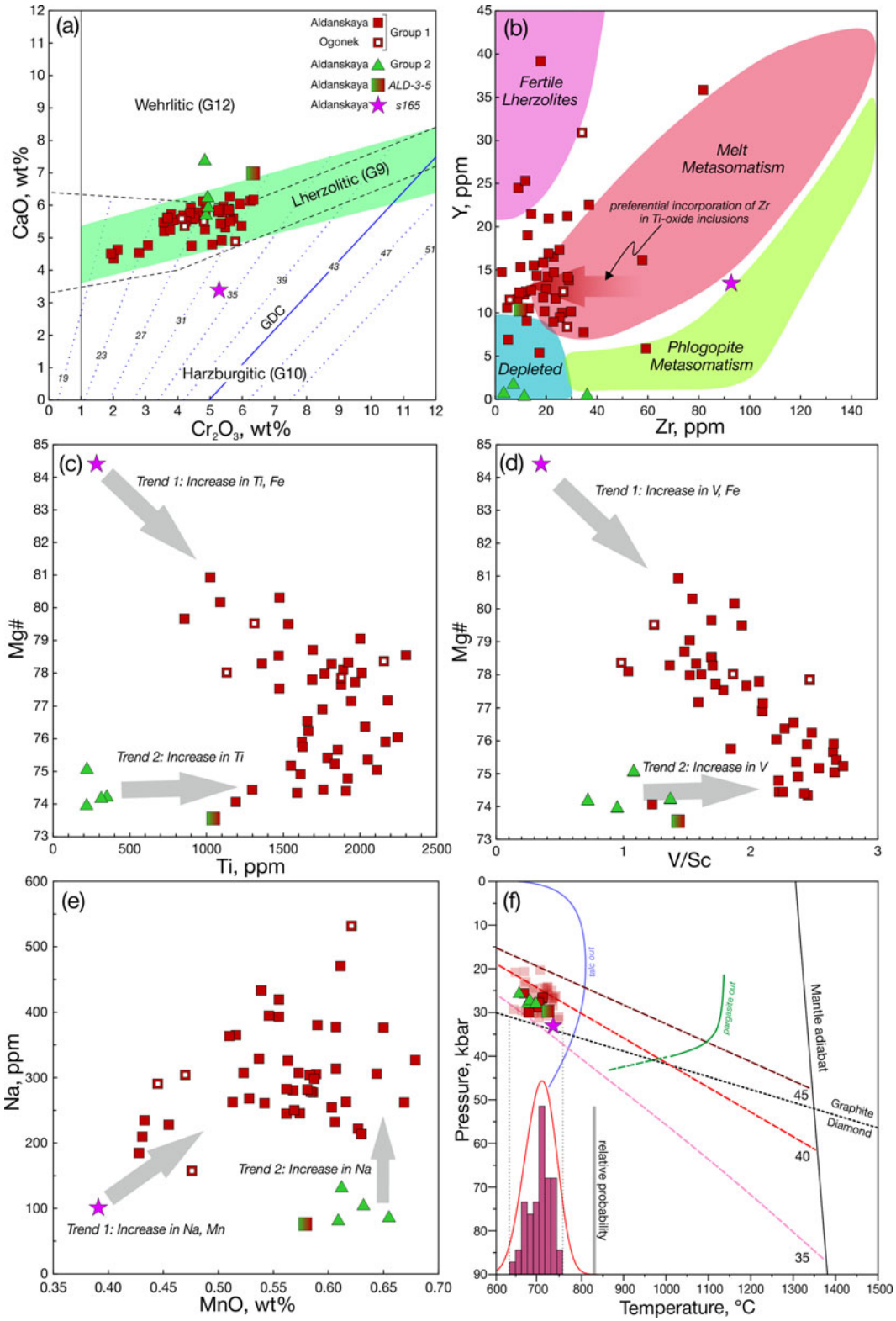

Fig. 4. Inter-element relationships (a–e) and *P–T* diagram (f) for Chompolo pyropes with oxide mineral inclusions. (a) Solid and dotted lines indicating fields for lherzolitic (G9), harzburgitic (G10) and wehrlitic (G12) garnets are after Grütter *et al.* (2004) and Sobolev *et al.* (1973), respectively. The isobars (in GPa) are after Grütter *et al.* (2006). (b) The Zr–Y plot showing fields for garnet from depleted, fertile and variably metasomatised sources is after Griffin and Ryan (1995). (c, d, e) Suggested enrichment trends discussed in the text. (f) The *P–T* diagram showing T_{Ni} estimates (Ryan *et al.*, 1996) combined with $P_{Cr/Ca}$ pressure values (Grütter *et al.*, 2006); samples showing minimal pressure values are transparent. The graphite-diamond transition line is after Day (2012). Model conductive geotherms and mantle adiabat are from Hasterok and Chapman (2011). The probability density plot with histogram was constructed via the Isoplot Add-In (Ludwig, 2003). Lavender blue line – talc stability field (Pawley and Wood, 1995), green line – pargasite stability field in a K-rich peridotite + CO_2 + H_2O system (Sweeney, 1994).

https://doi.org/10.1180/mgm.2021.89 Published online by Cambridge University Press

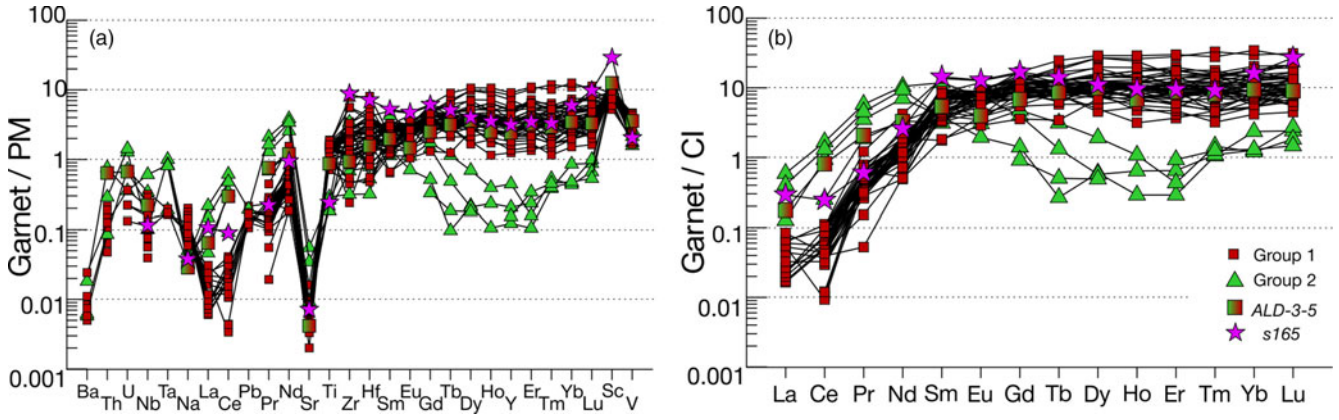

Fig. 5. Primitive mantle normalised (a) multi-element and (b) chondrite (C1) normalised REE distribution patterns of pyropes with oxide inclusions from the Chompolo lamprophyres. Normalisation values are from McDonough and Sun (1995).

pronounced harzburgitic (G10) affinity (Fig. 4a; Sobolev *et al.*, 1973; Grütter *et al.*, 2004). This xenocryst is akin to garnets of Group 1 in having normal REE patterns (though with a weakly sinusoidal trait; Fig 5b), whilst having very low Na (101 ppm) and Ti (289 ppm) concentrations similar to garnets of Group 2. Pyrope s165 has moderate Y (14 ppm) yet exhibits the highest Zr (93 ppm) among the xenocrysts investigated. Sample s165 is also extremely rich in Sc (471 ppm), which significantly exceeds the typical scandium abundances of peridotitic garnets (mostly in the range 75–200 ppm, median ~120 ppm; Chassé *et al.*, 2018). In the other Chompolo garnets investigated here, Sc abundances vary between 85 and 220 ppm. In addition, s165 is low in V (167 ppm), hence the V/Sc ratio of this grain (0.35) is much lower than that of the other xenocrysts (Fig. 4d).

Composition of the associated inclusions

Rutile

The TiO_2 concentration in rutile ranges from 89.3 to 96.7 wt.% (Supplementary Table S2). The rutile inclusions are enriched in Cr_2O_3 (0.61–7.21 wt.%), which is a characteristic feature of rutile derived from peridotitic mantle parageneses in on-craton settings (Malkovets *et al.*, 2016). In garnet ALD-1-9 the analysed rutile inclusions show variations in Cr_2O_3 abundances: two individual grains contain 0.61 and 3.03 wt.% Cr_2O_3, whereas rutile grains in two intergrowths with Mg-ilmenite in the same host contain 3.06 and 4.36 wt.% Cr_2O_3. Other substituting components in the rutile grains (wt.%) are FeO (0.55–2.93), V_2O_3 (up to 0.59), Al_2O_3 (up to 0.39), MgO (mostly < 0.10) and ZrO_2 (0.05–0.54). Other HFSE are negligible (<0.2 wt.% Nb_2O_5 and <0.1 wt.% Ta_2O_5).

Mg-rich ilmenite

The TiO_2 concentration in Mg-rich ilmenite varies from 51.3–57.5 wt.% (Supplementary Table S3). MgO shows variations from 8.3 to 15.1 wt.%. FeO_{total} is 24.4–35.5 wt.%. In common with rutile, Mg-ilmenite is characteristically Cr-rich (0.73–3.59 wt.% Cr_2O_3) and also varies in composition within a single pyrope host in sample ALD-1-9. Mg-rich ilmenite inclusions contain (wt.%) 0.07–0.28 V_2O_3, 0.07–0.49 Al_2O_3, 0.25–0.81 MnO and 0.05–0.41 NiO. High-field-strength elements (Nb, Ta and Zr) are < 0.1 wt.%. The ilmenite grains demonstrate intermediate compositions between ilmenite and geikielite with a minor hematite component. The compositional range for Mg-ilmenite in the Chompolo pyropes generally overlaps with Fe_2O_3-poor ilmenite compositions from peridotite xenoliths in kimberlites worldwide (e.g. Haggerty, 1991).

Crichtonite-group minerals

Crichtonite-group minerals are complex oxides with the general crystal-chemical formula $^{XII}A^{VI}B^{VI}C_{18}^{IV}T_2\Phi_{38}$, where major cations are: ^{XII}A = K, Ba, Sr, Ca, Na, LREE and Pb; ^{VI}B = Mn, Y, U, Fe, Zr, Sc and LREE; $^{VI}C_{18}$ = Ti, Fe, Cr, V, Nb, Mn and Al; $^{IV}T_2$ = Fe, Mg, Zn and Mn; Φ = O, (OH) and F (Roman numerals indicate the coordination numbers). The compositions of the crichtonite-group minerals studied are given in Supplementary Table S4. TiO_2 content ranges from 55.2 to 67.1 wt.%, Cr_2O_3 lies within 7.0–18.1 wt.%, MgO is between 3.26 and 4.40 wt.%. The dominant cations in ^{VI}C and ^{IV}T sites are Ti and Mg, respectively, and thus similar to other occurrences of crichtonite-series minerals reported in mantle-derived xenoliths (Haggerty *et al.*, 1983; Haggerty, 1991; Rezvukhin *et al.*, 2018). The B site is suggested to be dominated by either Fe (7.10–11.0 wt.% FeO) or Zr (1.54–5.41 wt.% ZrO_2). The grains investigated are enriched in Al (0.91–2.15 wt.% Al_2O_3), which occupies the ^{VI}C site together with Ti, Cr and Fe.

The dominant cations in the A site are Ca (20 analysed grains, 0.40–0.56 atoms per formula unit, apfu), Ba (5 grains; 0.35–0.82 apfu) and Sr (2 grains; 0.32 and 0.52 apfu). The occupancy of the A site in the crichtonite-group minerals studied is shown in Fig. 6a. The analysed grains form a trend from Ca- and Sr-rich compositions to the Ba apex of the diagram (Fig. 6a). Of significant interest are the intergrowths of crichtonite-group minerals with olivine and magnesite in sample s21 (Fig. 3i). Here the crichtonite-group minerals are relatively low in Ti (~56–57 wt.% TiO_2), contain high Cr_2O_3 (~16–17 wt.%), and are extremely rich in Ba (6.73–6.92 wt.% BaO). The amount of BaO in these grains almost reaches the highest reported concentration of BaO in a crichtonite-group mineral; a lindsleyite grain in a metasomatised harzburgite xenolith from the Boshof Road dumps, South Africa (7.14 wt.% BaO; Konzett *et al.*, 2013). A crichtonite-group mineral present in complex polymineralic inclusions (samples s291 and s317; Fig. 3k, l) is dominated by Sr in the A site and Fe in the B site. This mineral is botuobinskite, a new mineral species

https://doi.org/10.1180/mgm.2021.89 Published online by Cambridge University Press

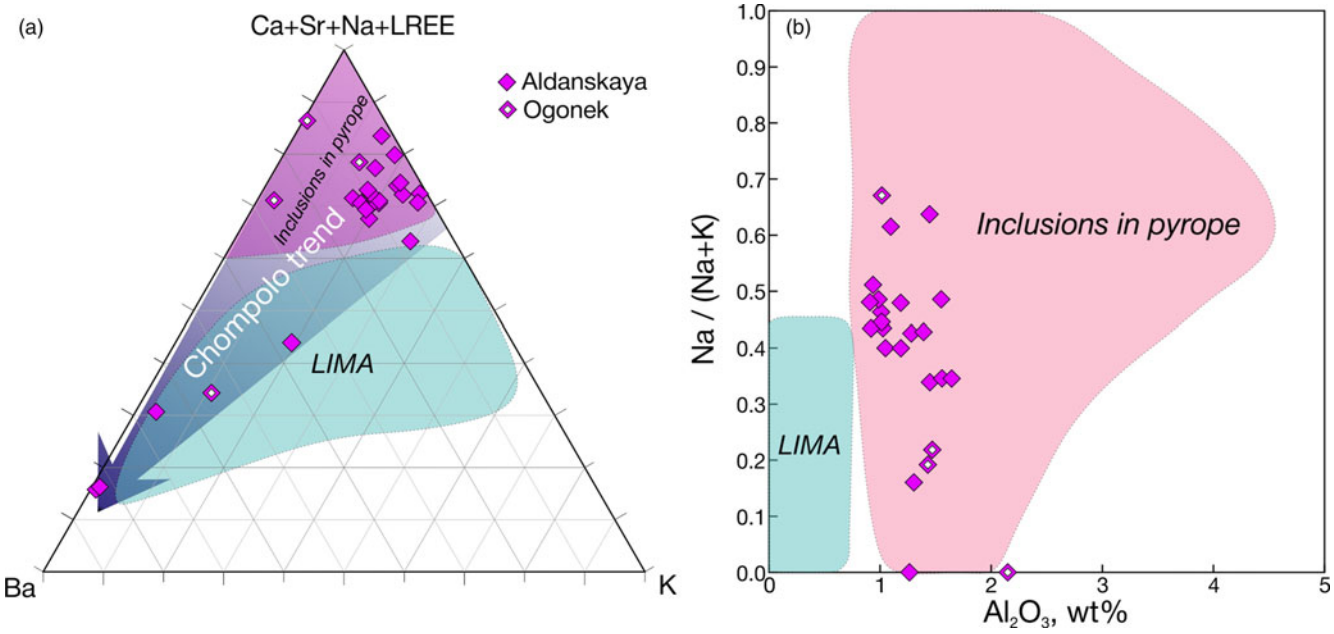

Fig. 6. (a) Ba–K–Ca+Sr+Na+LREE ternary diagram and (b) Al_2O_3–Na/(Na+K) binary plot showing compositions of inclusions of crichtonite-group minerals in Chompolo pyropes. 'LIMA' stands for lindsleyite–mathiasite series minerals in metasomatised peridotite xenoliths, mostly from South African kimberlites. Compositional fields for the 'LIMA' series and 'Inclusions in pyrope' are after (Rezvukhin *et al.*, 2018 and references therein). The 'Chompolo trend' shows enrichment of the crichtonite-group minerals from Chompolo pyropes in Ba – a feature that is not typical to crichtonite-group minerals as inclusions in pyropes from other localities.

of the crichtonite group introduced recently by Rezvukhin *et al.* (2020).

In Fig. 6b the Al_2O_3–Na/(Na+K) plot is designed to illustrate the compositional distinctions between the crichtonite-group minerals as inclusions in pyropes and K-rich Al-poor lindsleyite–mathiasite series minerals from metasomatised peridotite xenoliths (Rezvukhin *et al.*, 2018 and references therein). The grains investigated plot well within the field outlining the compositions of crichtonite-group minerals as inclusions in garnet. On average, the examined grains contain higher abundances of Na compared to lindsleyite–mathiasite series minerals (Fig. 6b).

The analytical totals of the crichtonite-group minerals vary from 96.5 to 100 wt.%; we infer that the crichtonite-group minerals with lower analytical sums contain increased proportions of Fe^{3+} and/or volatile component (mostly water). In particular, low analytical totals (~97–98 wt.%) were recorded for the crichtonite-group minerals in complex polymineralic inclusions where they are closely associated with water-bearing silicate minerals (phlogopite and amphibole) (Fig. 3k, l).

Cr-spinel

The Cr-spinel inclusions contain (wt.%) 8.10–12.9 MgO, 14.6–22.3 FeO, 2.43–6.54 Fe_2O_3, 45.0–58.8 Cr_2O_3, 7.25–19.7 Al_2O_3 and 0.19–0.31 MnO (Supplementary Table S5; Fe_2O_3 was calculated by stoichiometry after Droop, 1987). These are dominated either by the chromite ($FeCr_2O_4$) or magnesiochromite ($MgCr_2O_4$) components, with minor amounts of other end members. Spinel inclusions in Group 2 pyropes are slightly more aluminous on average than spinel in pyropes of the Group 1, whereas spinel in a specific xenocryst s165 has the most pronounced magnesiochromite composition among all the grains investigated. The spinel inclusions contain up to 1.4 wt.% TiO_2; enrichment in Ti is more characteristic to the spinel associated with Ti-oxides in Group 1 pyropes.

Other associated minerals

Olivine, diopside and enstatite inclusions are Mg-rich with Mg# varying from 90.3 to 93.6 (Supplementary Table S6). In diopside, Na_2O content ranges from 2.04 to 2.19 wt.%, Al_2O_3 is between 1.89 and 2.17 wt.%, and Cr_2O_3 is 1.8–2.0 wt.%, although in a diopside intergrowth with enstatite (sample ALD-1-4) contents of Na_2O, Al_2O_3 and Cr_2O_3 are as high as 3.31, 3.20 and 2.85 wt.%, respectively. Enstatite in the intergrowth with diopside (sample ALD-1-4) and an enstatite grain in a polymineralic inclusion (sample sx2) have roughly equal compositions with ~35.5 wt.% MgO and 4.59–4.84 wt.% FeO. TiO_2 in pyroxenes is low, not exceeding 0.16 wt.%. Phlogopite in polymineralic inclusions in pyropes s291 and s317 (Fig. 3k, l) shows high concentration of Ba (3.56–3.75 wt.% BaO). The calcic–alkaline amphibole in sample s291 is pargasite (according to Locock, 2014); it contains 9.82 wt.% CaO; 4.46 wt.% Na_2O and 1.05 wt.% K_2O. More detailed information on the occurrences and compositions of silicate, carbonate, sulfide and graphite inclusions in few samples from present study and in other Chompolo pyropes have been reported elsewhere (Nikolenko *et al.*, 2017, 2021; Sharygin *et al.*, 2017).

P–T estimates

Nickel concentrations in the pyrope crystals investigated are relatively low and vary in a narrow range of 8.9–16.3 ppm. The empirical Ni-in-garnet thermometer of Ryan *et al.* (1996) (T_{NiR96}) assumes equilibrium partitioning of Ni between pyrope and coexisting olivine. We consider T_{NiR96} to be applicable to the samples studied here, as pyropes display major-element

https://doi.org/10.1180/mgm.2021.89 Published online by Cambridge University Press

compositions typical for garnets of peridotitic affinity (Fig. 4a), and olivine has been recognised as an associated mineral in nine xenocrysts. When applied to the garnet suite, T_{NiR96} yields a temperature range of 640–750°C (±50°C).

The Cr/Ca-in-pyrope single-mineral barometer of Grütter *et al.* (2006) ($P_{Cr/Ca}$) was applied to 12 samples with Cr-spinel inclusions and yielded a pressure range of 25–33 kbar. This method requires equilibrium with Cr-spinel and assumes heat flow of 38 mW/m^2 (Grütter *et al.*, 2006). For other samples (without Cr-spinel inclusions) the minimum pressure values of 21–32 kbar were determined using $P_{Cr/Ca}$.

The application of conventional thermobarometry methods (detailed below) to garnet xenocrysts containing pyroxene inclusions (for which we had EMP data of good quality) proved ineffective because of the following reasons: (1) clinopyroxene grains do not pass the compositional filters established by Ziberna *et al.* (2016); (2) *P–T* values for the garnet suite are perhaps too low for reliable application of these methods; (3) it is possible that equilibration between the silicate minerals in question was not fully achieved. The temperatures estimated using three of four clinopyroxene inclusions are lower that the temperature range used for calibration of the enstatite-in-Cpx thermometer (850–1500°C; Nimis and Taylor, 2000), whereas orthopyroxene compositions yield highly inconsistent temperature values and unrealistically high pressure values at ~45–60 kbar using the Grt- and Opx-based thermobarometry methods commonly applied to mantle xenoliths (e.g. Nickel and Green, 1985; Brey and Köhler, 1990; Nimis and Grütter, 2010). Therefore, we consider that T_{NiR96} and $P_{Cr/Ca}$ provide the most reliable *P–T* estimates for the pyropes investigated.

The *P–T* values calculated using T_{NiR96} and $P_{Cr/Ca}$ place the samples just above the graphite–diamond transition line of Day (2012), consistent with a cold cratonic geotherm of 36–38 mW/m^2 (Fig. 4f). The xenocrysts appear to have been derived from low-temperature (~600–800°C) peridotite lithologies that resided in the graphite stability field (<110 km; 25–35 kbar; Fig. 4f), which is in agreement with the occurrence of graphite inclusions in Chompolo pyropes (this study, Nikolenko *et al.*, 2017). For previously studied inclusion-bearing Chompolo pyropes (featuring inclusions of graphite, sulfides and Cr-spinel), temperature assessments were calculated in the range of 640–910°C (Nikolenko *et al.*, 2017, 2020a, 2021). The occurrence of primary talc in the Chompolo samples does not contradict the *P–T* parameters obtained as talc is stable at the pressure range of 25–35 kbar up to ~800°C (e.g. Pawley and Wood, 1995).

Discussion

Origin of host pyropes

Pyropes of Group 1

Pyropes of Group 1 contain abundant Ti-rich oxide inclusions (rutile, Mg-rich ilmenite and crichtonite-group minerals), associated closely in intergrowths and composite polymineralic inclusions with hydrous silicate minerals, carbonates, sulfides and Cr-spinel. The compositions of the crichtonite-group minerals are characterised by a wide spectrum of incompatible elements (LILE, LREE, Zr), whereas REE distribution patterns of Group 1 pyropes exhibit enrichment in the MREE–HREE range. These modal and composition data as well as the trace-element abundances of the host pyropes allow us to conclude that Group 1 pyropes are metasomatic minerals that originated in the upper mantle beneath the Chompolo field as a result of peridotite protolith enrichment during the percolation of metasomatising fluids or melts. These metasomatic agents introduced a variety of incompatible elements as well as volatiles (H_2O, CO_2 S, P and Cl) necessary for the formation of hydrous silicate, carbonate and sulfide minerals.

The evidence concerning the metasomatic genesis of at least a proportion of Cr-pyropes in the lithospheric mantle of ancient cratons continues to grow (e.g. Shimizu and Richardson, 1987; Hoal *et al.*, 1994; Griffin and Ryan, 1995; Stachel *et al.*, 1998, 2004; Griffin *et al.*, 1999a; Aulbach *et al.*, 2004, 2013; Klein-BenDavid and Pearson, 2009; Agashev *et al.*, 2013; Howarth *et al.*, 2014; Rezvukhin *et al.*, 2018). It must be emphasised that Ti-oxide inclusions enriched in incompatible elements are characteristic only of Ca-rich pyropes of the lherzolitic paragenesis (Kostrovitsky and Garanin, 1992; Varlamov *et al.*, 1996; Wang *et al.*, 1999; Vrana, 2008; Rezvukhin *et al.*, 2016b, 2018), i.e. these inclusions are associated with lherzolite-style metasomatism (refertilisation) that occurred after melt-depletion events. The low-to-moderate concentrations of Zr in most Group 1 pyropes, plotting around the low-end of the 'melt metasomatism' trend proposed by Griffin and Ryan (1995) (Fig. 4b), at first glance might be evidence against the metasomatic enrichment process. However, it can be explained by the preferential distribution of Zr into associated Ti-oxide inclusions (rutile, ilmenite and especially crichtonite-group minerals containing up to 5.4 wt.% ZrO_2) during crystallisation. Such preferential fractionation moves garnet compositions from the field of 'melt metasomatism' to lower Zr concentrations (Fig. 4b). Previously, similar compositions of metasomatic garnets with inclusions of crichtonite-group minerals from the Internatsionalnaya kimberlite pipe were reported by Rezvukhin *et al.* (2018). Based on these data, we suggest that pyrope paragenesis in terms of associated titanate minerals should be taken into account when interpreting compositional features of Cr-pyrope in the Zr–Y space.

Pyropes of Group 2

Compared to Group 1, garnets of Group 2 show drastically different geochemical signatures. The latter exhibit much lower concentrations of Ti, V, Na, HREE and Y, and thus may be considered as ultra-depleted with regard to trace-element composition. Group 2 pyropes do not contain specific inclusions into which those elements could have fractionated; thus, depleted signatures are their distinctive primary feature. Interestingly, their Ca abundances are high (5.7–7.4 wt.% CaO) and correspond to the uppermost part of the lherzolite trend and to the lowermost part of the wehrlite field (Sobolev *et al.*, 1973; Grütter *et al.*, 2004) (Fig. 4a). These pyropes also exhibit elevated LREE in the La–Nd range. Hence, Group 2 pyropes show geochemical signatures of both strong depletion and enrichment. It appears that the metasomatic agent has not obliterated the effects of prior melt extraction to the same degree as in Group 1 lherzolitic garnets that have been thoroughly refertilised.

Literature data indicate that garnets similar to Group 2 represent a relatively abundant paragenetic type of pyrope in the lithospheric mantle; they appear to be relatively widespread in the Chompolo lithospheric mantle as well (Ashchepkov *et al.*, 2001). These pyropes comprise a particular compositional trend with higher Ca contents at given Cr concentration in comparison with the common lherzolite trend. They are present in worldwide kimberlites and lamprophyres of different ages (Kopylova *et al.*, 2000; Carbno and Canil, 2002; Aulbach *et al.*,

https://doi.org/10.1180/mgm.2021.89 Published online by Cambridge University Press

2004); on the Siberian craton they appear to be predominant in Mesozoic kimberlites (Tychkov *et al.*, 2008).

The affinity of pyropes with similar composition to spinel–garnet peridotite xenoliths (from Jericho kimberlite, Canada) led Kopylova *et al.* (2000) to the conclusion that their composition is controlled by equilibration with high-Cr deep-seated spinel (and clinopyroxene). This assumption is consistent with the occurrence of large Cr-spinel inclusions in Group 2 pyropes investigated here; however, it does not explain the extreme depletion in Ti, Na and Y. Carbno and Canil (2002) ascribed the origin of similar garnets to the percolation of metasomatic agents through an ultra-depleted peridotite protolith, which was also associated with heating. On the basis of the similarity between Ca–Cr compositional trends for these pyropes and pyroxenitic ones, and due to the increasing proportion of pyroxenitic pyropes in the Mezozoic Siberian kimberlites, Tychkov *et al.* (2008) further suggested that the origin of pyropes similar to Group 2 may be related to intrusions of high-temperature pyroxenitic magmas.

As Ca and LREE behave as incompatible elements during mantle processes, we assume that pyropes of Group 2 are clearly not the depleted residues (in a strict sense) of high degree partial melting. The high concentrations of Ca and LREE in Group 2 pyropes point to the involvement of these garnets in a metasomatic enrichment event. We speculate that Group 2 pyropes originated in the subcontinental lithospheric mantle beneath the Chompolo field due to percolation of a low-volume carbonated fluid or melt with a high LREE/HREE ratio through extremely depleted chromite-bearing peridotite protoliths. This metasomatic agent had probably equilibrated with a large volume of garnet in the deeper lithosphere (Aulbach *et al.*, 2013), which is consistent with high CaO, Ce/Yb and low TiO_2–Y–HREE abundances in Group 2 pyropes. High CaO concentrations that emplace some Group 2 samples well into the wehrlite field (Fig. 4a) are possible because the pyropes might have originally been derived from the harzburgite field but were retained at the lherzolite–wehrlite boundary *en route* to becoming 'genuine' wehrlitic garnets. The reason for this is probably the lack of Si in the agent necessary for the refertilisation reactions to proceed.

Xenocryst s165

Garnet s165 is the only pyrope that exhibits harzburgitic major-element composition. However, the REE distribution pattern of s165 can be considered as normal concave-upward, although it displays slightly elevated LREE and relatively depleted HREE in the Dy–Tm range (Fig. 5), which is probably the ancestral feature of its pre-existing sinuous shape. We argue that this sample is the least refertilised (by a little-fractionated silicate melt) and therefore the most refractory sample and closest in major-element composition to the original depleted residue (high Mg# and low Ti, Na and Mn). Therefore, it is the only harzburgitic sample in our collection which survived the extensive refertilisation and fractionated melt metasomatism but which has nonetheless been cryptically metasomatised.

The highest Zr concentration among the samples (93 ppm) together with moderate Y (14 ppm) places s165 on the border between 'melt metasomatism' and 'phlogopite metasomatism' compositional trends (Griffin and Ryan, 1995) (Fig. 4b). The occurrence of talc and phlogopite inclusions reflects the involvement of a water-rich metasomatic agent in the formation of this sample. Chassé *et al.* (2018) have demonstrated recently that volatile-rich fluid metasomatism positively affects Sc concentrations in mantle garnet. Thus, the extremely high Sc (470 ppm), of this sample probably reflects the effect of such metasomatism. In contrast, the high content of Zr in s165 in some respects contradicts with the fluid-related nature of metasomatism, as Zr is a conservative element which is more mobile in melts than in volatile-rich fluids (Pearce and Peate, 1995). We assume that s165 has undergone the effect of material from two sources superimposed on an ultra-depleted protolith and which perhaps was also recrystallised. The initial source (fluid?) contributed to the elevated LREE, Sc and the formation of inclusions of hydrous silicate minerals, whereas the second (melt?) added M–HREE and Zr. Alternatively, this metasomatic agent was a low-volume volatile-rich melt that had undergone little fractionation. Contrary to Group 2 samples, the high Y-HREE contents of s165 suggest that the metasomatic agent(s) had not interacted extensively with the garnet-bearing matrix, perhaps consistent with formation at the highest pressure for this sample inferred from the CaO–Cr_2O_3 relationships (Fig. 4f).

Are garnets of different groups related to each other?

The Ti–Mg#, V/Sc–Mg# and MnO–Na (Fig. 4c–e) relationships imply that garnets of Group 1 may represent evolved products of metasomatism superimposed on garnets of Group 2 and a garnet suite corresponding in composition to sample s165. The hypothetical 'trend 1' may have been responsible for the transformation of s165 type pyropes into Group 1 pyropes with the addition of Ca, Fe, Ti, V, Na and Mn. Note that these elements are the major constituents of the crichtonite-group minerals, which are abundant as inclusions in garnets of Group 1. Similarly, 'trend 2' has been responsible for the transformation of Group 2 pyropes into Group 1 pyropes with the addition of Ti, V, Na and HREE. A good example of the 'trend 2' effect is sample ALD-3-5 that exhibits intermediate composition between Group 1 and Group 2 (Fig. 2g; Fig. 4; Supplementary Table S1).

It is also interesting to note that s165 and Group 2 samples display low V/Sc ratios, whereas Group 1 xenocrysts comprise well-defined trends towards higher V/Sc ratios (Fig. 4d). Vanadium is a multivalent trace element that can be used as a redox sensor, and becomes more incompatible in typical mantle minerals with increasing oxygen fugacity (Mallmann and O'Neill, 2009; Aulbach *et al.*, 2017; Woodland *et al.*, 2018). The V–Sc relationships of the pyropes indicate that Group 1 xenocrysts crystallised under relatively reducing conditions, whereas the low V/Sc ratios of the more refractory s165 and Group 2 grains point to the involvement of more oxidising metasomatic agents.

Origin of elongated oxide inclusions

A significant controversy surrounds the origin of Ti-oxide needles in Cr-pyrope as the criteria to distinguish epigenetic inclusions from syngenetic ones are not obvious. As a rule, elongated oxide inclusions in Cr-pyrope are oriented along specific crystallographic directions (Alifirova *et al.*, 2012, 2020; Wang *et al.*, 1999; Vrana, 2008; Rezvukhin *et al.*, 2018, 2019). Two mechanisms have been suggested for the origin of oriented inclusions in garnet namely syngenetic (epitaxial co-precipitation) and epigenetic (solid-state isochemical exsolution). A number of considerations allow us to argue against an exsolution origin for the oxide inclusions investigated here, these are: (1) inclusion textures differ from those of typical exsolution, as pyropes commonly contain several dozen inclusions that may be distributed unevenly in the pyrope host, and the grains (Figs 2, 3) are significantly larger

https://doi.org/10.1180/mgm.2021.89 Published online by Cambridge University Press

than the fine lamellae typically observed as exsolution products; (2) pyrope xenocrysts enclose abundant crichtonite-group minerals, which are enriched in a wide spectrum of incompatible elements and are considered to be typical metasomatic phases in the lithospheric mantle (e.g. Haggerty, 1991; Kalfoun *et al.*, 2002; Konzett *et al.*, 2013); (3) mantle garnets contain extremely low levels of Ba (e.g. Aulbach *et al.*, 2017), so the exsolution of Ba-rich crichtonite-group minerals from the mantle garnet is highly unlikely; (4) some Ti-rich oxides vary in composition within individual pyrope grains (e.g. in sample ALD-1-9); differences in composition between lamellae are abnormal for exsolution (e.g. Dawson, 2004); (5) all the oxide minerals investigated (rutile, ilmenite, crichtonite-group minerals and Cr-spinel) occur in complex polymineralic inclusions (intergrowths), which undoubtedly have primary origin and might represent trapped and subsequently crystallised droplets of fluid or melt. Such polymineralic aggregates comprising oxide, silicate, carbonate and sulfide minerals have been reported in pyrope grains from other localities (Wang *et al.*, 1999; Vrana, 2008; Rezvukhin *et al.*, 2018). All of the above evidence indicates that inclusions of Ti-rich oxides and silicate, carbonate and sulfide minerals were formed syngenetically with the host garnet from the parental fluid or melt phase(s).

Comparison with oxide inclusions in pyropes from other localities and Ti-oxides in mantle metasomatic associations

Inclusions in pyropes from the Chompolo lamprophyres represent a typical set of high-Ti and/or Cr-rich oxides, reported previously in Cr-pyrope from kimberlite and lamprophyre bodies of the Siberian craton (Botkunov *et al.*, 1987; Kostrovitsky and Garanin, 1992; Varlamov *et al.*, 1996; Alifirova *et al.*, 2012, 2020; Ziberna *et al.*, 2013; Rezvukhin *et al.*, 2016a, 2016b, 2018; Nikolenko *et al.*, 2017), ultramafic magmatic breccias of the Colorado Plateau, USA (Wang *et al.*, 1999), and European peridotite massifs (Săbău and Alberico, 2003; Vrana, 2008). These minerals are also common as xenocrysts in kimberlites and components of metasomatised peridotite xenoliths worldwide (e.g. Haggerty, 1991).

However, we note several prominent compositional features in the Chompolo inclusions of rutile and crichtonite-group minerals. Rutile is a typical storage site of HFSE (Nb, Ta, Zr and Hf) both in eclogites (Rudnick *et al.*, 2000; Aulbach *et al.*, 2008) and metasomatised peridotites (Haggerty, 1991; Ionov *et al.*, 1999; Grégoire *et al.*, 2000; Kalfoun *et al.*, 2002; Konzett *et al.*, 2013). Rutile inclusions in pyropes from the Garnet Ridge diatreme, Colorado Plateau (Wang *et al.*, 1999) and Internatsionalnaya kimberlite pipe, Siberian craton (Rezvukhin *et al.*, 2016b) were reported to be enriched in HFSE (Nb, Zr and Ta). Rezvukhin *et al.* (2016b) emphasised that ~40% of the rutile inclusions contained >1 wt.% Nb_2O_5, up to a maximum of 15.6 wt.%. Rutile in metasomatised peridotite xenoliths sampled by kimberlites of the Kaapvaal craton is also enriched in Nb_2O_5 (e.g. Jones *et al.*, 1982; Schulze, 1990; Konzett *et al.*, 2013), and this enrichment is extremely pronounced in rutile from metasomatised nodules from the Orapa kimberlite, Botswana (up to 20.9 wt.% Nb_2O_5; Tollo and Haggerty, 1987). High concentrations of Nb and Zr were established in rutile from metasomatic veins and pockets in spinel peridotite xenoliths sampled by alkali basalts in off-cratonic environments (e.g. Ionov *et al.*, 1999; Grégoire *et al.*, 2000; Kalfoun *et al.*, 2002). However, Nb and Ta abundances are low in rutile and crichtonite-group minerals analysed in this work (commonly <0.1 wt.% Nb_2O_5 and Ta_2O_5). For the Ti-rich oxides investigated the indicative HFSE is Zr rather than Nb or Ta.

The crichtonite-group minerals studied here from Chompolo show a major trend from Ca–Sr-rich to Ba-rich compositions (Fig. 6a). The Ca- and Sr-rich varieties are similar in composition to the crichtonite-group mineral inclusions in pyropes from other localities, e.g. ultramafic diatreme of the Garnet Ridge cluster, Colorado Plateau (Wang *et al.*, 1999) and Internatsionalnaya kimberlite pipe, Siberian craton (Rezvukhin *et al.*, 2018). In the Chompolo pyropes, we have recognised the occurrence of botuobinskite, a recently discovered Sr^{A}-Fe^{B}-dominant species of the crichtonite group (holotype sample from the Internatsionalnaya pipe; Rezvukhin *et al.*, 2020). Ba-rich species are close in composition to the lindsleyite–mathiasite solid-solution series (Ba- and K-dominant members of the group, respectively), reported in metasomatised peridotite xenoliths in South African and Chinese kimberlites (e.g. Jones *et al.*, 1982; Haggerty *et al.*, 1983; Haggerty, 1991; Lu and Zhou, 1994; Konzett *et al.*, 2013). However, the lindsleyite–mathiasite series is lower in Al (<1 wt.% Al_2O_3; Fig. 6b) and may contain significant Nb_2O_5 exceeding 1.5 wt.% (Lu and Zhou, 1994; Konzett *et al.*, 2013).

The composition and origin of the metasomatic agent(s), comparison with other localities

The present research offers an inclusion-based approach to constrain the nature and composition of the metasomatic phase(s) responsible for the formation of the samples investigated. This relies on the general composition of associated minerals, especially the inclusions of the crichtonite-group species as well as the modal composition of the polymineralic inclusions, which might represent trapped and subsequently crystallised droplets of the parental fluid/melt phase.

During recent decades, mantle-derived titanates have received increased attention due to their petrological and geochemical significance for various mantle processes (Haggerty *et al.*, 1986; Haggerty, 1991; Kalfoun *et al.*, 2002; Bulanova *et al.*, 2004). Crichtonite-group minerals are capable of hosting a wide spectrum of silicate-incompatible elements (LILE, HFSE and REE) and thus may serve as essential reservoirs for trace elements in the upper mantle. Their origin from liquids enriched in incompatible elements provides important constraints on the composition of these at the time of crystallisation. Compositional characteristics of the crichtonite-group minerals and other Ti-rich oxides investigated (rutile and Mg-ilmenite) indicate that the metasomatic phase(s) responsible for the crystallisation of pyropes with such inclusions contained significant Ti, Zr, V, LILE (Ba, Sr), Ca, K, Na and LREE (La, Ce).

The characteristic enrichment in Cr_2O_3 in crichtonite-group minerals, rutile, Mg-rich ilmenite, spinel and host pyrope is attributed to the Cr-rich nature of mantle peridotites. Chromium and magnesium were inherited from peridotite protoliths, where they were stored as relatively immobile elements in (magnesio)chromite and perhaps pre-existing depleted garnet (Haggerty *et al.*, 1986; Rezvukhin *et al.*, 2018), and were subsequently redistributed during a metasomatic overprint. Enrichment in Al_2O_3 is a characteristic feature of crichtonite-group minerals as inclusions in garnet worldwide (Fig. 6b), and which might be explained by the equilibration with Al-rich garnet.

The abundance of water-bearing silicates, carbonates, sulfides, graphite and apatite in Chompolo pyropes (more than 15 minerals; Nikolenko *et al.*, 2017, 2021; Sharygin *et al.*, 2017; Alifirova

https://doi.org/10.1180/mgm.2021.89 Published online by Cambridge University Press

et al., 2020; this study) indicates that the fluid/melt also contained significant volatile components (H_2O, CO_2, S, P and Cl). The monomineralic and polymineralic inclusions investigated here are similar to the associations found in pyropes from ultramafic diatremes of the Navajo volcanic field, Colorado plateau (McGetchin and Silver, 1970; Hunter and Smith, 1981; Smith, 1987, 2020; Wang *et al.*, 1999). The eruption of several diatremes (Garnet Ridge, Red Mesa, Moses Rock and others) within the Colorado Plateau at ca. 30–24 Ma resulted from hot upwelling during subduction of the Farallon plate beneath northwestern America (Dickinson, 1997; Usui *et al.*, 2003; Smith, 2020). For the pyropes from the Garnet Ridge diatreme, which enclose abundant Ti-rich oxide, carbonate and water-bearing inclusions, an origin in a metasomatised mantle wedge overlying a subducted slab was proposed (Wang *et al.*, 1999). By contrast, pyrope xenocrysts sampled by the Internatsionalnaya kimberlite magma at the Siberian craton core (Mirny kimberlite field) characterised by very thick diamondiferous lithosphere, do not show such remarkable inclusion mineralogy (Rezvukhin *et al.*, 2018). For these samples, the most abundant inclusions are oxides and sulfides, yet carbonates, apatite, graphite, water-bearing minerals and composite intergrowths of these phases occur far less commonly (Rezvukhin *et al.*, 2018). The comparison of samples suggests that the metasomatic agent from which the Internatsionalnaya samples crystallised was relatively volatile-poor whereas the inclusion-rich Chompolo and Navajo garnets originated from volatile-enriched liquids.

Observations on mode and compositions of the inclusions as well as the paragenetic links to other occurrences indicated above, imply that the formation of the pyrope xenocrysts might be related to large-scale subduction processes. Over its prolonged history, the eastern Asia region has experienced a number of major subduction events which were manifested by ubiquitous intraplate magmatism, metasomatic events, earthquakes and continental lithosphere destruction (e.g. Zonenshain *et al.*, 1990; Maruyama *et al.*, 1997; Van der Voo *et al.*, 1999; Parfenov *et al.*, 2011; Li and van der Hilst, 2010; Zhu *et al.*, 2012; Safonova and Santosh, 2014; Liu *et al.*, 2017). The subduction of the Mongol–Okhotsk branch of the Palaeo-Pacific beneath Siberia, which probably initiated in Middle–Late Palaeozoic (see Donskaya *et al.*, 2013 and references therein), is one of the possible scenarios which generated the reworking of mantle lithologies beneath the Central Aldan. In contrast, based on isotopic data, Bogatikov *et al.* (1994), Davies *et al.* (2006) and Nikolenko *et al.* (2020b) assumed the ancient (Precambrian) subduction zones gave rise to the metasomatic enrichment of the source regions of Aldan alkaline magmas, thus implying a major break between the development of the source regions and the Mesozoic eruption of alkaline melts. It also should be noted that Velikoslavinsky *et al.* (2006, 2011) proposed the Palaeoproterozoic (ca. 2.0–1.9 Ga) geodynamic system of the active continental margin of the Olekma–Aldan continental microplate and the Fedorov island arc for the central Aldan.

Thus, it may have been one of the Palaeo-subduction systems that triggered the intensive metasomatic effects on the lithospheric mantle associations beneath the Aldan shield by slab-derived fluids or melts, which were responsible for the crystallisation of inclusion-bearing pyropes. Similar conclusions regarding the role of subduction in the metasomatic modification of peridotites from Tok (Aldan shield) were reached by Ionov *et al.* (2005). In such a scenario the subducted oceanic slab was the major source of volatile-enriched metasomatic agents, which subsequently modified the peridotitic lithologies of the overlying mantle wedge. The abundance of primary talc, phlogopite and amphibole in Chompolo pyropes proves the hydrous nature of the involved fluids or melts. The significance of talc for H_2O recycling in subduction zones has been postulated previously by Pawley and Wood (1995). The spatial relationship of the Central Aldan to the subduction zones might account for the similarities between the Chompolo mantle assemblages and the inclusion associations in the pyropes (and in other minerals) from various occurrences located closely to the convergent plate margins. Grains of metasomatic pyrope resided within the host peridotites until they were sampled subsequently as xenoliths and xenocrysts by the Chompolo magmas in the Mesozoic during the lithosphere reactivation processes. These processes governed the magma eruptions within the Aldan alkaline province and in turn may have been caused by subduction. The Aldan alkaline magmas are mostly of lamproitic affinity and feature the pronounced enrichment in incompatible elements (K, Ti, Al, Rb, Sr, Zr and Ba) typical of lamproites. It appears that at the time of lamproite and lamprophyre magmatism, the Aldan lithospheric mantle was a very metasomatised (refertilised) region of the Siberian craton and a major source of incompatible elements for the generation of mantle melts.

Implications for Earth's volatile cycle and ore-forming processes

The Aldan shield forms part of the global inventory of severely disturbed cratonic lithosphere with reduced depths to the lithosphere–asthenosphere boundary relative to the intact Siberian craton interior (Aulbach, 2018 and references therein). The emplacement of volatiles in such a disturbed lithosphere might form an important part of Earth's volatile cycles (Gibson *et al.*, 2020). The Chompolo assemblages feature volatile-enriched minerals that are not common in pyropes derived from the inner parts of the Siberian craton (Rezvukhin *et al.*, 2018). In particular, Chompolo pyropes encompass sulfide minerals, talc, phlogopite, amphibole, apatite, graphite and carbonate. Further extension would exhume these volatile-bearing assemblages to shallower depths and might cause further formation of volatile-rich magmas that consume the volatile-bearing minerals and release sulfur currently bound in sulfide minerals, which may be critical to ore formation processes.

According to Holwell *et al.* (2019), ore deposits probably represent key depositional points along the mantle to upper-crust pathway taken by the magmas and hydrothermal fluids, effectively resulting from a magmatic–hydrothermal continuum. In this regard, the incompatible element-enriched metasomatised mantle beneath the Aldan shield appears to have exerted an important control on the origin of major ore deposits (U, Au, Mo, PGE and rare metals) formed from the Early Precambrian to Late Mesozoic. It is of importance that Late Mesozoic economically-valuable mineral systems on the Aldan shield are characterised by a close spatial–temporal association with alkaline mantle-derived magmas (Khomich *et al.*, 2015). The lithospheric mantle metasomatism that generated a pronounced diversity of minerals rich in incompatible elements and volatiles in the mantle sections such as those beneath Chompolo is probably an intermediate link between slab dehydration and formation of productive ore systems within the crust.

Summary

The present study contributes to the investigation of poorly-described mantle parageneses beneath the Chompolo area,

https://doi.org/10.1180/mgm.2021.89 Published online by Cambridge University Press

Aldan shield, southeastern Siberian craton. The research deals with inclusion assemblages in mantle Cr-rich pyropes with emphasis on Ti- and Cr-rich oxide phases. The primary mineral inclusion suite includes rutile, Mg-ilmenite, crichtonite-group minerals and Cr-spinel, which are associated within host pyropes with silicates, carbonates, sulfides, graphite and apatite. The major- and trace-element compositions of host garnets and inclusions link pyrope origin to metasomatic processes in the lithospheric mantle beneath the Chompolo field. Inclusions of Ti-rich oxides in association with hydrous minerals, carbonates and sulfides imply that the formation of Cr-pyropes encapsulating such inclusions occurred in the Chompolo lithospheric mantle with the participation of metasomatising melts or fluids enriched in volatiles (H_2O, CO_2, S, P and Cl) and incompatible elements (Ti, Zr, V, Ba, Sr, K, Na, Ca and REE). Inter-element relationships suggest the effects of two distinct metasomatic sources. The first was responsible for the addition of Ca, Fe, Ti, V, Na and Mn and the second introduced Ti, V, Na and HREE. The metasomatic agents were volatile-rich melts or supercritical C–O–H–S fluids with possible genetic affinities to a subduction environment. High concentrations of Cr_2O_3 in pyropes and inclusions are attributed to the Cr-rich nature of peridotite protoliths. Due to the established diversity of minerals enriched in incompatible elements and volatiles, these conclusions have implications for the models of ore formation and global volatile cycles.

Acknowledgements. This study was supported by the grant of the President of the Russian Federation (MK-971.2020.5) to DIR. The authors received additional funding from the Russian Science Foundation grant No. 18-77-10062 (SEM-EDS data and BSE imagery). Fieldworks on the Aldan shield and sampling were performed within the state assignment project of IGM SB RAS.

LA-ICP-MS study in the analytical centre 'Geoanalitik' was supported by the state assignment of the 'Geoanalitik' shared research facilities of IGG UB RAS (No. AAAA-A18-118053090045-8). The re-equipment and comprehensive development of the 'Geoanalitik' shared research facilities of IGG UB RAS is supported financially by the grant of the Ministry of Science and Higher Education of the Russian Federation (Agreement No. 075-15-2021-680). We thank Roger Mitchell, Makoto Arima and Helen Kerbey for efficient editorial handling. Sonja Aulbach and an anonymous reviewer provided valuable and incisive comments that improved the quality of the report.

Supplementary material. To view supplementary material for this article, please visit https://doi.org/10.1180/mgm.2021.89

References

Agashev A.M., Ionov D.A., Pokhilenko N.P., Golovin A.V., Cherepanova Y. and Sharygin I.S. (2013) Metasomatism in lithospheric mantle roots: Constraints from whole-rock and mineral chemical composition of deformed peridotite xenoliths from kimberlite pipe Udachnaya. *Lithos*, **160–161**, 201–215.

Alifirova T.A., Pokhilenko L.N., Ovchinnikov Y.I., Donnelly C.L., Riches A.J.V. and Taylor L.A. (2012) Petrologic origin of exsolution textures in mantle minerals: evidence in pyroxenitic xenoliths from Yakutia kimberlites. *International Geology Review*, **54**, 1071–1092.

Alifirova T., Rezvukhin D., Nikolenko E., Pokhilenko L., Zelenovskiy P., Sharygin I., Korsakov A. and Shur V. (2020) Micro-Raman study of crichtonite group minerals enclosed into mantle garnet. *Journal of Raman Spectroscopy*, **51**, 1493–1512.

Ashchepkov I.V., Vladykin N.V., Saprykin A.I., Khmelnikova O.S. and Anoshin G.N. (2001) Composition and thermal structure of the mantle in peripheral parts of Siberian craton. *Revista Brasileira de Geociências*, **31**, 527–536.

Aulbach S. (2018) Cratonic lithosphere discontinuities: dynamics of small-volume melting, metacratonization, and a possible role for brines. Pp. 177–203 in: *Lithospheric Discontinuities, Geophysical Monograph 239* (H. Yuan and B. Romanowicz, editors).

Aulbach S., Griffin W.L., O'Reilly S.Y. and McCandless T.E. (2004) Genesis and evolution of the lithospheric mantle beneath the Buffalo Head Terrane, Alberta (Canada). *Lithos*, **77**, 413–451.

Aulbach S., O'Reilly S.Y., Griffin W.L. and Pearson N.J. (2008) Subcontinental lithospheric mantle origin of high niobium/tantalum ratios in eclogites. *Nature Geoscience*, **1**, 468–472.

Aulbach S., Griffin W.L., Pearson N.J. and O'Reilly S.Y. (2013) Nature and timing of metasomatism in the stratified mantle lithosphere beneath the central Slave craton (Canada). *Chemical Geology*, **352**, 153–169.

Aulbach S., Sun J., Tappe S., Höfer H.E. and Gerdes A. (2017) Volatile-rich metasomatism in the cratonic mantle beneath SW Greenland: link to kimberlites and mid-lithospheric discontinuities. *Journal of Petrology*, **58**, 2311–2338.

Bogatikov O.A., Ryabchikov I.D., Kononova V.A., Makhotkin I.L., Novgorodova N.I., Solovova I.P., Galuskin E.V., Ganeev I.I., Girnis A.V. and Eremeev N.V. (1991) *Lamproites*. Priroda, Moscow, pp. 302.

Bogatikov O.A., Kononova V.A., Pervov V.A. and Zhuravlev D.Z. (1994) Petrogenesis of Mesozoic potassic magmatism of the Central Aldan: a Sr-Nd isotopic and geodynamic model. *International Geology Review*, **36**, 629–644.

Botkunov A.I., Garanin V.K., Krot A.N. and Kudryavtseva G.P. (1987) Mineral inclusions in garnets from kimberlites of Yakutia: their genetic and practical significance. *International Geology Review*, **29**, 163–177.

Boyd F.R. (1989) Compositional distinction between oceanic and cratonic lithosphere. *Earth and Planetary Science Letters*, **96**, 15–26.

Brey G.P. and Köhler T. (1990) Geothermobarometry in four-phase lherzolites II. New thermobarometers, and practical assessment of existing thermobarometers. *Journal of Petrology*, **31**, 1353–1378.

Bulanova G.P., Muchemwa E., Pearson D.G., Griffin B.J., Kelley S.P., Klemme S. and Smith C.B. (2004) Syngenetic inclusions of yimengite in diamond from Sese kimberlite (Zimbabwe) – evidence for metasomatic conditions of growth. *Lithos*, **77**, 181–192.

Canil D., Schulze D.J., Hall D., Hearn B.C. and Milliken S.M. (2003) Lithospheric roots beneath western Laurentia: the geochemical signal in mantle garnets. *Canadian Journal of Earth Sciences*, **40**, 1027–1051.

Carbno G.B. and Canil D. (2002) Mantle structure beneath the SW Slave craton, Canada: Constraints from garnet geochemistry in the Drybones Bay kimberlite. *Journal of Petrology*, **43**, 129–142.

Chassé M., Griffin W.L., Alard O., O'Reilly S.Y. and Calas G. (2018) Insights into the mantle geochemistry of scandium from a meta-analysis of garnet data. *Lithos*, **310**, 409–421.

Davies G.R., Stolz A.J., Mahotkin I.L., Nowell G.M. and Pearson D.G. (2006) Trace element and Sr–Pb–Nd–Hf isotope evidence for ancient, fluid-dominated enrichment of the source of Aldan Shield lamproites. *Journal of Petrology*, **47**, 1119–1146.

Dawson J.B. (2004) A fertile harzburgite-gamet lherzolite transition: possible inferences for the roles of strain and metasomatism in upper mantle peridotites. *Lithos*, **77**, 553–569.

Dawson J.B. and Stephens W. (1975) Statistical classification of garnets from kimberlite and associated xenoliths. *The Journal of Geology*, **1975**, 589–607.

Day H.W. (2012) A revised diamond-graphite transition curve. *American Mineralogist*, **97**, 52–62.

Dickinson W.R. (1997) Overview: Tectonic implications of Cenozoic volcanism in coastal California. *Geological Society of America Bulletin*, **109**, 936–954.

Donskaya T.**V.** (2020) Assembly of the Siberian craton: constraints from Paleoproterozoic granitoids. *Precambrian Research*, **348**, 105869.

Donskaya T.V., Gladkochub D.P., Mazukabzov A.M. and Ivanov A.V. (2013) Late Paleozoic–Mesozoic subduction-related magmatism at the southern margin of the Siberian continent and the 150 million-year history of the Mongol-Okhotsk Ocean. *Journal of Asian Earth Sciences*, **62**, 79–97.

Doucet L.S., Ionov D.A., Golovin A.V. and Pokhilenko N.P. (2012) Depth, degrees and tectonic settings of mantle melting during craton formation: inferences from major and trace element compositions of spinel harzburgite xenoliths from the Udachnaya kimberlite, central Siberia. *Earth and Planetary Science Letters*, **359–360**, 206–218.

Droop G.T.R. (1987) A general equation for estimating Fe3+ concentrations in ferromagnesian silicates and oxides from microprobe analyses, using stoichiometric criteria. *Mineralogical Magazine*, **51**, 431–435.

Gibson S.A., Rooks E.E., Day J.A., Petrone C.M. and Leat P.T. (2020) The role of sub-continental mantle as both "sink" and "source" in deep Earth volatile cycles. *Geochimica et Cosmochimica Acta*, **275**, 140–162.

Grégoire M., Lorand J.P., O'Reilly S.Y. and Cottin J.Y. (2000) Armalcolite-bearing, Ti-rich metasomatic assemblages in harzburgitic xenoliths from the Kerguelen Islands: Implications for the oceanic mantle budget of high-field strength elements. *Geochimica et Cosmochimica Acta*, **64**, 673–694.

Griffin W.L. and Ryan C.G. (1995) Trace elements in indicator minerals: area selection and target evaluation in diamond exploration. *Journal of Geochemical Exploration*, **53**, 311–337.

Griffin W.L., Fisher N.I., Friedman J., Ryan C.G. and O'Reilly S.Y. (1999a) Cr-pyrope garnets in the lithospheric mantle. I. Compositional systematics and relations to tectonic setting. *Journal of Petrology*, **40**, 679–704.

Griffin W.L., Ryan C.G., Kaminsky F.V., O'Reilly S.Y., Natapov L.M., Win T.T., Kinny P.D. and Ilupin I.P. (1999b) The Siberian lithosphere traverse: mantle terranes and the assembly of the Siberian Craton. *Tectonophysics*, **310**, 1–35.

Griffin W.L., Shee S.R., Ryan C.G., Win T.T. and Wyatt B.A. (1999c) Harzburgite to lherzolite and back again: metasomatic processes in ultramafic xenoliths from the Wesselton kimberlite, Kimberley, South Africa. *Contributions to Mineralogy and Petrology*, **134**, 232–250.

Griffin W.L., O'Reilly S.Y., Abe N., Aulbach S., Davies R.M., Pearson N.J., Doyle B.J. and Kivi K. (2003) The origin and evolution of Archean lithospheric mantle. *Precambrian Research*, **127**, 19–41.

Griffin W.L., Powell W.J., Pearson N.J. and O'Reilly S.Y. (2008) GLITTER: data reduction software for laser ablation ICP-MS. Pp. 204–207 in: *Laser Ablation-ICP-MS in the Earth Sciences*. Mineralogical Association of Canada short course series, **40**.

Grütter H.S., Gurney J.J., Menzies A.H. and Winter F. (2004) An updated classification scheme for mantle-derived garnet, for use by diamond explorers. *Lithos*, **77**, 841–857.

Grütter H., Latti D. and Menzies A. (2006) Cr-saturation arrays in concentrate garnet compositions from kimberlite and their use in mantle barometry. *Journal of Petrology*, **47**, 801–820.

Grütter H.S., Pell J.A. and Fitzgerald C.E. (2018) Use of a simplified Mahalanobis distance approach to constrain the dispersion and provenance of Cr-pyrope populations at the Chidliak kimberlite province, Nunavut, Canada. *Mineralogy and Petrology*, **112**, 707–718.

Gurney J.J. and Switzer G.S. (1973) The discovery of garnets closely related to diamonds in the Finsch pipe, South Africa. *Contributions to Mineralogy and Petrology*, **39**, 103–116.

Gurney J.J. and Zweistra P. (1995) The interpretation of the major element compositions of mantle minerals in diamond exploration. *Journal of Geochemical Exploration*, **53**, 293–309.

Haggerty S.E. (1991) Oxide mineralogy of the upper mantle. Pp. 355–416 in: *Oxide Minerals: Petrologic and Magnetic Significance* (D.H. Lindsley, editor). Reviews in Mineralogy, **Vol. 25**. Mineralogical Society of America, Washington DC.

Haggerty S.E., Smyth J.R., Erlank A.J., Rickard R.S. and Danchin R.V. (1983) Lindsleyite (Ba) and mathiasite (K): two new chromium-titanates in the crichtonite series from the upper mantle. *American Mineralogist*, **68**, 494–505.

Haggerty S.E., Erlank A.J. and Grey I.E. (1986) Metasomatic mineral titanate complexing in the upper mantle. *Nature*, **319**, 761–763.

Hasterok D. and Chapman D. (2011) Heat production and geotherms for the continental lithosphere. *Earth and Planetary Science Letters*, **307**, 59–70.

Hoal K.E.O., Hoal B.G., Erlank A.J. and Shimizu N. (1994) Metasomatism of the mantle lithosphere recorded by rare earth elements in garnets. *Earth and Planetary Science Letters*, **126**, 303–313.

Holwell D.A., Fiorentini M., McDonald I., Lu Y., Giuliani A., Smith D.J., Keith M. and Locmelis M. (2019) A metasomatized lithospheric mantle control on the metallogenic signature of post-subduction magmatism. *Nature Communications*, **10**, 1–10.

Howarth G.H., Barry P.H., Pernet-Fisher J.F., Baziotis I.P., Pokhilenko N.P., Pokhilenko L.N., Bodnar R.J., Taylor L.A. and Agashev A.M. (2014) Superplume metasomatism: Evidence from Siberian mantle xenoliths. *Lithos*, **184–187**, 209–224.

Hunter W.C. and Smith D. (1981) Garnet peridotite from Colorado Plateau ultramafic diatremes: hydrates, carbonates, and comparative geothermometry. *Contributions to Mineralogy and Petrology*, **76**, 312–320.

Ionov D.A., Gregoire M. and Prikhod'ko V.S. (1999) Feldspar–Ti-oxide metasomatism in off-cratonic continental and oceanic upper mantle. *Earth and Planetary Science Letters*, **165**, 37–44.

Ionov D.A., Prikhodko V.S., Bodinier J.L., Sobolev A.V. and Weis D. (2005) Lithospheric mantle beneath the south-eastern Siberian craton: petrology of peridotite xenoliths in basalts from the Tokinsky Stanovik. *Contributions to Mineralogy and Petrology*, **149**, 647–665.

Ivanov A.V., Vladykin N.V., Demonterova E.I., Gorovoy V.A. and Dokuchits E.Y. (2018) 40Ar/39Ar geochronology of the Malyy (Little) Murun massif, Aldan shield of the Siberian craton: A simple story for an intricate igneous complex. *Minerals*, **8**, 602.

Jaques A.L., Lewis J.D., Smith C.B., Gregory G.P., Ferguson J., Chappell B.W. and McCulloch M.T. (1984) The diamond-bearing ultrapotassic (lamproitic) rocks of the West Kimberley region, Western Australia. *Developments in Petrology*, **11**, 225–254.

Jones A.P., Smith J.V. and Dawson J.B. (1982) Mantle metasomatism in 14 veined peridotites from Bultfontein mine, South Africa. *The Journal of Geology*, **90**, 435–453.

Kalfoun F., Ionov D. and Merlet C. (2002) HFSE residence and Nb/Ta ratios in metasomatised, rutile-bearing mantle peridotites. *Earth and Planetary Science Letters*, **199**, 49–65.

Khomich V.G., Boriskina N.G. and Santosh M. (2015) Geodynamics of late Mesozoic PGE, Au, and U mineralization in the Aldan shield, North Asian Craton. *Ore Geology Reviews*, **68**, 30–42.

Klein-BenDavid O. and Pearson D.G. (2009) Origins of subcalcic garnets and their relation to diamond forming fluids – Case studies from Ekati (NWT-Canada) and Murowa (Zimbabwe). *Geochimica et Cosmochimica Acta*, **73**, 837–855.

Kobussen A.F., Griffin W.L. and O'Reilly S.Y. (2009) Cretaceous thermochemical modification of the Kaapvaal cratonic lithosphere, South Africa. *Lithos*, **112**, 886–895.

Konzett J., Wirth R., Hauzenberger C. and Whitehouse M. (2013) Two episodes of fluid migration in the Kaapvaal Craton lithospheric mantle associated with Cretaceous kimberlite activity: evidence from a harzburgite containing a unique assemblage of metasomatic zirconium-phases. *Lithos*, **182–183**, 165–184.

Kopylova M.G., Russell J.K., Stanley C. and Cookenboo H. (2000) Garnet from Cr- and Ca-saturated mantle: implications for diamond exploration. *Journal of Geochemical Exploration*, **68**, 183–199.

Kornilova V. (1997) Petrography and mineralogy of the calc-alkaline lamprophyres and eruptive breccias from Chompolo area. *Otechestvennaya Geologiya,* **9**, 6–9.

Kostrovitsky S.I. and Garanin V.K. (1992) High-chromium titanates in pyropes of the Aldanskaya dyke (Yakutia). *Zapiski Vsesoyuznogo Mineralogicheskogo Obshchestva*, **121**, 67–71.

Laetsch T. and Downs R.T. (2006) Software for identification and refinement of cell parameters from powder diffraction data of minerals using the RRUFF Project and American Mineralogist Crystal Structure Databases. Abstract Pp. 23–28 in: *19th General Meeting of the International Mineralogical Association*. Kobe, Japan.

Lafuente B., Downs R., Yang H. and Stone N. (2015) The power of databases: The RRUFF project. Pp. 1–30 in: *Highlights in Mineralogical Crystallography* (T. Armbruster and R.M. Danisi, editors). De Gruyter, Berlin.

Li C. and van der Hilst R.D. (2010) Structure of the upper mantle and transition zone beneath Southeast Asia from traveltime tomography. *Journal of Geophysical Research: Solid Earth*, **115**.

Liu X., Zhao D., Li S. and Wei W. (2017) Age of the subducting Pacific slab beneath East Asia and its geodynamic implications. *Earth and Planetary Science Letters*, **464**, 166–174.

Locock A.J. (2014) An Excel spreadsheet to classify chemical analyses of amphiboles following the IMA 2012 recommendations. *Computers & Geosciences*, **62**, 1–11.

https://doi.org/10.1180/mgm.2021.89 Published online by Cambridge University Press

Lu Q. and Zhou H. (1994) A new progress in research on mathiasite in Mengying, Shandong, III. Oxide minerals containing the large ions Cr, Ti and Fe in the upper mantle. *Acta Mineralogica Sinica*, **14**, 343–347.

Ludwig K.R. (2003) *Isoplot 3.00: A Geochronological Toolkit for Microsoft Excel*, Berkeley Geochronology Center Special Publication Vol. 4. Berkeley Geochronology Center, California, USA.

Makhotkin I., Arakelyants M. and Vladykin N. (1989) On the age of lamproites from the Aldanian province. *Doklady Akademii Nauk SSSR*, **306**, 703–707.

Malkovets V.G., Griffin W.L., O'Reilly S.Y. and Wood B.J. (2007) Diamond, subcalcic garnet, and mantle metasomatism: Kimberlite sampling patterns define the link. *Geology*, **35**, 339–342.

Malkovets V.G., Rezvukhin D.I., Belousova E.A., Griffin W.L., Sharygin I.S., Tretiakova I.G., Gibsher A.A., O'Reilly S.Y., Kuzmin D.V., Litasov K.D., Logvinova A.M., Pokhilenko N.P. and Sobolev N.V. (2016) Cr-rich rutile: A powerful tool for diamond exploration. *Lithos*, **265**, 304–311.

Mallmann G. and O'Neill H.S.C. (2009) The crystal/melt partitioning of V during mantle melting as a function of oxygen fugacity compared with some other elements (Al, P, Ca, Sc, Ti, Cr, Fe, Ga, Y, Zr and Nb). *Journal of Petrology*, **50**, 1765–1794.

Maruyama S., Isozaki Y., Kimura G. and Terabayashi M. (1997) Paleogeographic maps of the Japanese Islands: plate tectonic synthesis from 750 Ma to the present. *Island Arc*, **6**, 121–142.

McDonough W.F. and Sun S.S. (1995) The composition of the Earth. *Chemical Geology*, **120**, 223–253.

McGetchin T.R. and Silver L.T. (1970) Compositional relations in minerals from kimberlite and related rocks in the Moses Rock dike, San Juan County, Utah. *American Mineralogist*, **55**, 1738–1771.

McLean H., Banas A., Creighton S., Whiteford S., Luth R.W. and Stachel T. (2007) Garnet xenocrysts from the Diavik mine, NWT, Canada: composition, color, and paragenesis. *The Canadian Mineralogist*, **45**, 1131–1145.

Mitchell R., Smith C. and Vladykin N. (1994) Isotopic composition of strontium and neodymium in potassic rocks of the Little Murun complex, Aldan Shield, Siberia. *Lithos*, **32**, 243–248.

Mues-Schumacher U., Keller J., Kononova V. and Suddaby P. (1995) Petrology and age determinations of the ultramafic (lamproitic) rocks from the Yakokut complex, Aldan Shield, Eastern Siberia. *Mineralogical Magazine*, **59**, 409–428.

Mues-Schumacher U., Keller J., Kononova V.A. and Suddaby P.J. (1996) Mineral chemistry and geochronology of the potassic alkaline ultramafic Inagli complex, Aldan Shield, eastern Siberia. *Mineralogical Magazine*, **60**, 711–730.

Nickel K. and Green D. (1985) Empirical geothermobarometry for garnet peridotites and implications for the nature of the lithosphere, kimberlites and diamonds. *Earth and Planetary Science Letters*, **73**, 158–170.

Nikolenko E.I., Sharygin I.S., Alifirova T.A., Korsakov A.V., Zelenovskiy P.S. and Shur V.Y. (2017) Graphite-bearing mineral assemblages in the mantle beneath Central Aldan superterrane of North Asian craton: combined confocal micro-Raman and electron microprobe characterization. *Journal of Raman Spectroscopy*, **48**, 1597–1605.

Nikolenko E., Sharygin I., Malkovets V., Rezvukhin D. and Afanasiev V. (2020a). Mineralogy and geochemistry of the inclusion-bearing Cr-pyropes from the Chompolo lamprophyres, Aldan shield, Siberian craton. Abstract id 12823 in: *EGU General Assembly Conference Abstracts*. Vienna, Austria, 4–8 May 2020.

Nikolenko E.I., Lobov K.V., Agashev A.M., Tychkov N.S., Chervyakovskaya M.V., Sharygin I.S. and Nikolenko A.M. (2020b) 40Ar/39Ar geochronology and new mineralogical and geochemical data from lamprophyres of Chompolo field (South Yakutia, Russia). *Minerals*, **10**, 886.

Nikolenko E.I., Sharygin I.S., Rezvukhin D.I., Malkovets V.G., Tychkov N.S. and Pokhilenko N.P. (2021) Sulfide-bearing polymineralic inclusions in mantle-derived garnets from lamprophyres of the Chompolo field (Central Aldan, Siberian craton). *Doklady Earth Sciences*, **497**, 300–304.

Nimis P. and Grütter H. (2010) Internally consistent geothermometers for garnet peridotites and pyroxenites. *Contributions to Mineralogy and Petrology*, **159**, 411–427.

Nimis P. and Taylor W.R. (2000) Single clinopyroxene thermobarometry for garnet peridotites. Part I. Calibration and testing of a Cr-in-Cpx barometer and an enstatite-in-Cpx thermometer. *Contributions to Mineralogy and Petrology*, **139**, 541–554.

Paquette J.-L., Ionov D.A., Agashev A.M., Gannoun A. and Nikolenko E.I. (2017) Age, provenance and Precambrian evolution of the Anabar shield from U-Pb and Lu-Hf isotope data on detrital zircons, and the history of the northern and central Siberian craton. *Precambrian Research*, **301**, 134–144.

Parfenov L.M., Berzin N.A., Badarch G., Belichenko V.G., Bulgatov A.N., Dril S.I., Khanchuk A.I., Kirillova G.L., Kuz'min M.I., Nokleberg W.J., Ogasawara M., Obolenskiy A.A., Prokopiev A.V., Rodionov S.M., Scotese C.R., Timofeev V.F., Tomurtogoo O. and Yan H. (2011) Tectonic and metallogenic model for Northeast Asia. in: *Metallogenesis and Tectonics of Northeast Asia* (W.J. Nokleberg, editor). US Department of the Interior, US Geological Survey.

Pawley A.R. and Wood B.J. (1995) The high-pressure stability of talc and 10 Å phase: potential storage sites for H_2O in subduction zones. *American Mineralogist*, **80**, 998–1003.

Pearce J.A. and Peate D.W. (1995) Tectonic implications of the composition of volcanic arc magmas. *Annual Review of Earth and Planetary Sciences*, **23**, 251–285.

Pokhilenko N.P., Sobolev N.V., Kuligin S.S. and Shimizu N. (1999). Peculiarities of distribution of pyroxenite paragenesis garnets in Yakutian kimberlites and some aspects of the evolution of the Siberian craton lithospheric mantle. Pp. 689–698 in: *Proceedings of the 7th International Kimberlite Conference*. Cape Town, South Africa.

Prokopyev I., Doroshkevich A., Ponomarchuk A., Redina A., Yegitova I., Ponomarev J., Sergeev S., Kravchenko A., Ivanov A. and Sokolov E. (2019) 1U-Pb SIMS and Ar-Ar geochronology, petrography, mineralogy and gold mineralization of the late Mesozoic Amga alkaline rocks (Aldan shield, Russia). *Ore Geology Reviews*, **109**, 520–534.

Rezvukhin D.I., Malkovets V.G., Sharygin I.S., Kuzmin D.V., Gibsher A.A., Litasov K.D., Pokhilenko N.P. and Sobolev N.V. (2016a) Inclusions of crichtonite group minerals in pyropes from the Internatsionalnaya kimberlite pipe, Yakutia. *Doklady Earth Sciences*, **466**, 206–209.

Rezvukhin D.I., Malkovets V.G., Sharygin I.S., Kuzmin D.V., Litasov K.D., Gibsher A.A., Pokhilenko N.P. and Sobolev N.V. (2016b) Inclusions of Cr-and Cr–Nb-Rutile in pyropes from the Internatsionalnaya kimberlite pipe, Yakutia. *Doklady Earth Sciences*, **466**, 173–176.

Rezvukhin D.I., Malkovets V.G., Sharygin I.S., Tretiakova I.G., Griffin W.L. and O'Reilly S.Y. (2018) Inclusions of crichtonite-group minerals in Cr-pyropes from the Internatsionalnaya kimberlite pipe, Siberian Craton: Crystal chemistry, parageneses and relationships to mantle metasomatism. *Lithos*, **308–309**, 181–195.

Rezvukhin D.I., Alifirova T.A., Korsakov A.V. and Golovin A.V. (2019) A new occurrence of yimengite-hawthorneite and crichtonite-group minerals in an orthopyroxenite from kimberlite: Implications for mantle metasomatism. *American Mineralogist*, **104**, 761–774.

Rezvukhin D.I., Rashchenko S.V., Sharygin I.S., Malkovets V.G., Alifirova T.A., Pautov L.A., Nigmatulina E.N. and Seryotkin Y.V. (2020) Botuobinskite, IMA 2018-143a. CNMNC Newsletter 57, CNMNC Newsletter No. 57; *Mineralogical Magazine*, 84, https://doi.org/10.1180/mgm.2020.73

Rosen O.M. and Turkina O.M. (2007) The oldest rock assemblages of the Siberian Craton. Pp. 793–838 in: *Developments in Precambrian Geology* (K.C Condie, editor). Elsevier.

Rosen O.M., Condie K.C., Natapov L.M. and Nozhkin A.D. (1994) Archean and Early Proterozoic evolution of the Siberian craton: a preliminary assessment. Pp. 411–459 in: *Archean Crustal Evolution* (K.C. Condie, editor). Elsevier, Amsterdam.

Rudnick R.L., Barth M., Horn I. and McDonough W.F. (2000) Rutile-bearing refractory eclogites: Missing link between continents and depleted mantle. *Science*, **287**, 278–281.

Ryan C.G., Griffin W.L. and Pearson N.J. (1996) Garnet geotherms: Pressure-temperature data from Cr-pyrope garnet xenocrysts in volcanic rocks. *Journal of Geophysical Research*, **101**, 5611–5625.

Săbău G. and Alberico A. (2003). A new loveringite occurrence: Oriented rods in garnet from the Foltea lherzolite, South Carpathians, Romania. Pp. 92 in: *2nd Mineral Sciences in the Carpathians International Conference*. Szeged, Hungary.

https://doi.org/10.1180/mgm.2021.89 Published online by Cambridge University Press

Safonova I.Y. and Santosh M. (2014) Accretionary complexes in the Asia-Pacific region: tracing archives of ocean plate stratigraphy and tracking mantle plumes. *Gondwana Research*, **25**, 126–158.

Schulze D.J. (1989) Constraints on the abundance of eclogite in the upper mantle. *Journal of Geophysical Research: Solid Earth*, **94**, 4205–4212.

Schulze D.J. (1990) Silicate-bearing rutile-dominated nodules from South African kimberlites: Metasomatized cumulates. *American Mineralogist*, **75**, 97–104.

Scully K.R., Canil D. and Schulze D.J. (2004) The lithospheric mantle of the Archean Superior Province as imaged by garnet xenocryst geochemistry. *Chemical Geology*, **207**, 189–221.

Sharygin I.S., Nikolenko E.I. and Lobov K.V. (2017). Carbonate inclusions in Cr-pyropes derived from the mantle beneath Central Aldan superterrane of Siberian cratonin. Abstract No. 11IKC-4606 in: *International Kimberlite Conference: Extended Abstracts,* 11. Gaborone, Botswana.

Shchukina E.V., Agashev A.M. and Pokhilenko N.P. (2016) Metasomatic origin of garnet xenocrysts from the V. Grib kimberlite pipe, Arkhangelsk region, NW Russia. *Geoscience Frontiers*, **8**, 641–651.

Shilina G. and Zeitlin S. (1959) On the first finding of kimberlites in Aldan. *Soviet Geology*, **10**, 132–136.

Shimizu N. and Richardson S. (1987) Trace element abundance patterns of garnet inclusions in peridotite-suite diamonds. *Geochimica et Cosmochimica Acta*, **51**, 755–758.

Shirey S.B., Cartigny P., Frost D.J., Keshav S., Nestola F., Nimis P., Pearson D.G., Sobolev N.V. and Walter M.J. (2013) Diamonds and the geology of mantle carbon. Pp. 355–421 in: *Carbon in Earth* (R.M. Hazen, A.P. Jones and J.A. Baross, editors). Reviews in Mineralogy & Geochemistry, **75**. Mineralogical Society of America and the Geochemical Society, Chantilly, Virginia, USA.

Smelov A.P. and Timofeev V.F. (2005). The tectonics and metallogeny of the Precambrian of the Aldan-Stanovoy Shield. Pp. 53–56 in: *Mineral Deposit Research: Meeting The Global Challenge*. Springer, Berlin, Heidelberg, Germany.

Smelov A.P. and Timofeev V.F. (2007) The age of the North Asian Cratonic basement: an overview. *Gondwana Research*, **12**, 279–288.

Smelov A.P., Shatsky V.S., Ragozin A.L., Reutskii V.N. and Molotkov A.E. (2012) Diamondiferous Archean rocks of the Olondo greenstone belt (western Aldan–Stanovoy shield). *Russian Geology and Geophysics*, **53**, 1012–1022.

Smith D. (1987) Genesis of carbonate in pyrope from ultramafic diatremes on the Colorado Plateau, southwestern United States. *Contributions to Mineralogy and Petrology*, **97**, 389–396.

Smith D. (2020) Trace elements in Cr-pyrope from the Navajo volcanic field of the Colorado Plateau, SW USA, and implications for the mantle wedge during low-angle subduction. *Lithos*, **362–363**, 105460, doi: 10.1016/j.lithos.2020.105460.

Smith B.H.S. and Skinner E.M.W. (1984) A new look at Prairie Creek, Arkansas. *Developments in Petrology*, **11**, 255–283.

Sobolev N.V., Lavrent'ev Y.G., Pokhilenko N.P. and Usova L.V. (1973) Chrome-rich garnets from the kimberlites of Yakutia and their parageneses. *Contributions to Mineralogy and Petrology*, **40**, 39–52.

Stachel T. and Harris J.W. (2008) The origin of cratonic diamonds – constraints from mineral inclusions. *Ore Geology Reviews*, **34**, 5–32.

Stachel T., Viljoen K.S., Brey G. and Harris J.W. (1998) Metasomatic processes in lherzolitic and harzburgitic domains of diamondiferous lithospheric mantle: REE in garnets from xenoliths and inclusions in diamonds. *Earth and Planetary Science Letters*, **159**, 1–12.

Stachel T., Aulbach S., Brey G.P., Harris J.W., Leost I., Tappert R. and Viljoen K.S. (2004) The trace element composition of silicate inclusions in diamonds: a review. *Lithos*, **77**, 1–19.

Sweeney R.J. (1994) Carbonatite melt compositions in the Earth's mantle. *Earth and Planetary Science Letters*, **128**, 259–270.

Tollo R.P. and Haggerty S.E. (1987) Nb-Cr-rutile in the Orapa kimberlite pipe, Botswana. *The Canadian Mineralogist*, **25**, 251–264.

Tommasi A., Vauchez A. and Ionov D.A. (2008) Deformation, static recrystallization, and reactive melt transport in shallow subcontinental mantle xenoliths (Tok Cenozoic volcanic field, SE Siberia). *Earth and Planetary Science Letters*, **272**, 65–77.

Tychkov N.S., Pokhilenko N.P., Kuligin S.S. and Malygina E.V. (2008) Composition and origin of peculiar pyropes from lherzolites: evidence for the evolution of the lithospheric mantle of the Siberian Platform. *Russian Geology and Geophysics*, **49**, 225–239.

Usui T., Nakamura E., Kobayashi K., Maruyama S. and Helmstaedt H. (2003) Fate of the subducted Farallon plate inferred from eclogite xenoliths in the Colorado Plateau. *Geology*, **31**, 589–592.

Van der Voo R., Spakman W. and Bijwaard H. (1999) Mesozoic subducted slabs under Siberia. *Nature*, **397**, 246–249.

Varlamov D.A., Garanin V.K. and Kostrovitskiy S.I. (1996) Exotic high-titanium minerals as inclusions in garnets from lower crustal and mantle xenoliths. *Transactions of the Russian Academy of Sciences, Earth Science Section,* **345A**, 352–355.

Velikoslavinskii S.D., Kotov A.B., Tolmacheva E.V., Sal'nikova E.B., Kovach V.P. and Larin A.M. (2011) Early Precambrian granite-gneiss complexes in the Central Aldan Shield. *Petrology*, **19**, 382–398.

Velikoslavinsky S.D., Kotov A.B., Sal'nikova E.B., Kovach V.P., Glebovitsky V.A., Zagornaya N.Y., Yakovleva S.Z., Tolmacheva E.V., Anisimova I.V. and Fedoseenko A.M. (2006) Protoliths of the metamorphic rocks of the Fedorov Complex, Aldan Shield: character, age, and geodynamic environments of origin. *Petrology*, **14**, 21–38.

Vladimirov N., Dauev Y. and Zubarev B. (1989) *Geology and Genesis of Diamond Deposits*. TsNIGRI, Moscow, Russia.

Vladykin N.V. (1997) Geochemistry and genesis of lamproites of the Aldan Shield. *Russian Geology and Geophysics*, **38**, 128–141.

Vladykin N. (2009) Potassium alkaline lamproite-carbonatite complexes: petrology, genesis, and ore reserves. *Russian Geology and Geophysics*, **50**, 1119–1128.

Vrana S. (2008) Mineral inclusions in pyrope from garnet peridotites, Kolín area, central Czech Republic. *Journal of Geosciences*, **53**, 17–30.

Walter M.J. (1998) Melting of garnet peridotite and the origin of komatiite and depleted lithosphere. *Journal of Petrology*, **39**, 29–60.

Wang L., Essene E.J. and Zhang Y. (1999) Mineral inclusions in pyrope crystals from Garnet Ridge, Arizona, USA: implications for processes in the upper mantle. *Contributions to Mineralogy and Petrology*, **135**, 164–178.

Woodland A., Uenver-Thiele L. and Seitz H. (2018) Influence of metasomatism on vanadium-based redox proxies for mantle peridotite. *Geochemical Perspectives Letters*, **8**, 11–16.

Zaitsev A.I. and Smelov A.P. (2010) *Isotope Geochronology of Kimberlite Rocks of the Yakutian Province*. Ofset, Yakutsk, Russia, Pp. 108.

Zhu R.-X., Yang J.-H. and Wu F.-Y. (2012) Timing of destruction of the North China Craton. *Lithos*, **149**, 51–60.

Zhu R.Z., Ni P., Ding J.Y., Wang G.G., Fan M.S. and Li S.N. (2019) Metasomatic processes in the Lithospheric mantle beneath the No. 30 Kimberlite (Wafangdian Region, North China Craton). *The Canadian Mineralogist*, **57**, 499–517.

Ziberna L., Nimis P., Zanetti A., Marzoli A. and Sobolev N.V. (2013) Metasomatic processes in the central Siberian cratonic mantle: Evidence from garnet xenocrysts from the Zagadochnaya kimberlite. *Journal of Petrology*, **54**, 2379–2409.

Ziberna L., Nimis P., Kuzmin D. and Malkovets V.G. (2016) Error sources in single-clinopyroxene thermobarometry and a mantle geotherm for the Novinka kimberlite, Yakutia. *American Mineralogist*, **101**, 2222–2232.

Zonenshain L.P., Kuzmin M.I. and Natapov L.M. (1990) *Geology of the USSR: a Plate-Tectonic Synthesis*. American Geophysical Union, Washington.

https://doi.org/10.1180/mgm.2021.89 Published online by Cambridge University Press